



**Understanding Interactions of Organic Nitrates with the
Surface and Bulk of Organic Films: Implications for Particle
Growth in the Atmosphere**

Journal:	<i>Environmental Science: Processes & Impacts</i>
Manuscript ID	EM-ART-08-2018-000348.R1
Article Type:	Paper
Date Submitted by the Author:	16-Oct-2018
Complete List of Authors:	<p>Vander Wall, Allison; University of California, Irvine, Department of Chemistry Lakey, Pascale; University of California, Irvine, Department of Chemistry Rossich-Molina, Estefania; Hebrew University of Jerusalem - Edmond J Safra Campus, Chemistry Perraud, Veronique; University of California, Chemistry Wingen, Lisa; University of California, Chemistry Xu, Jing; Institute of Theoretical Chemistry, Jilin University, Changchun 130023, People's Republic of China., ; Chemistry Soulsby, David; University of Redlands, Chemistry Department Gerber, Robert; The Hebrew University of Jerusalem , Chemistry; University of California, Irvine, Shiraiwa, Manabu; University of California, Irvine, Chemistry Finlayson-Pitts, Barbara; University of California, Irvine, Department of Chemistry</p>

1
2
3 1 Understanding Interactions of Organic Nitrates with the Surface and Bulk of
4 2 Organic Films: Implications for Particle Growth in the Atmosphere
5 3
6 4
7 5
8 6
9 7
10 8
11 9
12 10
13 11
14 12
15 13
16 14
17 15
18 16
19 17
20 18
21 19
22 20
23 21
24 22
25 23
26 24
27 25
28 26
29 27
30 28
31 29
32 30
33 31
34 32
35 33
36 34
37 35
38 36
39 37
40 38
41 39
42 40
43 41
44 42
45 43
46 44
47 45
48 46
49 47
50 48
51 49
52 50
53 51
54 52
55 53
56 54
57 55
58 56
59 57
60 58

A. C. Vander Wall,[†] P. S. J. Lakey,[†] E. Rossich-Molina,[‡] V. Perraud,[†] L. M. Wingen,[†] J. Xu,[†] D. Soulsby,^{††} R. B. Gerber,^{‡†*} M. Shiraiwa,^{†*} and B. J. Finlayson-Pitts^{†*}

[†]Department of Chemistry
University of California, Irvine
Irvine, CA 92697, USA

^{††}Department of Chemistry
University of Redlands
1200 East Colton Ave
Redlands, CA 92373, USA

[‡]Institute of Chemistry, Fritz Haber Research Center
Hebrew University of Jerusalem
Jerusalem 91904, Israel

October 16, 2018

Revision for:

Environmental Science: Processes and Impacts

*Corresponding authors: For experiments, bjfinlay@uci.edu; phone: (949) 824-7670; FAX: (949) 824-2420; for structure characterization, bgerber@uci.edu; for kinetic modeling, m.shiraiwa@uci.edu.

UptakePaperText_101618_revised.doc

30 **Abstract**

31 Understanding impacts of secondary organic aerosol (SOA) in air requires a molecular-level
32 understanding of particle growth via interactions between gases and particle surfaces. The
33 interactions of three gaseous organic nitrates with selected organic substrates was measured at
34 296 K using attenuated total reflection Fourier transform infrared spectroscopy. The organic
35 substrates included a long chain alkane (triacontane, TC), a keto-acid (pinonic acid, PA), an
36 amorphous ester oligomer (poly(ethylene adipate), PEA), and laboratory-generated SOA from α -
37 pinene ozonolysis. There was no uptake of the organic nitrates on the non-polar TC substrate, but
38 significant uptake occurred on PEA, PA, and α -pinene SOA. Net uptake coefficients (γ) at the
39 shortest reaction times accessible in these experiments ranged from 3×10^{-4} to 9×10^{-6} and
40 partition coefficients (K) from 1×10^7 to 9×10^4 . Trends in γ did not quantitatively follow trends in
41 K, suggesting that the intermolecular forces involved in gas-surface interactions are not the same
42 as those in the bulk, which is supported by theoretical calculations. Kinetic modeling showed
43 that nitrates diffused throughout the organic films over several minutes, and that the bulk
44 diffusion coefficients evolved as uptake/desorption occurred. A plasticizing effect occurred
45 upon incorporation of the organic nitrates, whereas desorption caused decreases in diffusion
46 coefficients in the upper layers, suggesting a crusting effect. Accurate predictions of particle
47 growth in the atmosphere will require knowledge of uptake coefficients, which are likely to be
48 several orders of magnitude less than one, and of the intermolecular interactions of gases with
49 particle surfaces as well as with the particle bulk.

1
2
3 **51 Environmental Significance**
4
5

6 52 The size and composition of atmospheric particles affects their light-scattering properties and
7
8 53 ability to act as cloud condensation nuclei, which in turn affects Earth's radiative balance.
9

10 54 Understanding how gases are taken up into particles to grow them to larger sizes is essential for
11
12 55 accurately predicting their effects. This study shows that net uptake coefficients for unreactive
13
14 56 gases such as organic nitrates into model organic substrates can be several orders of magnitude
15
16 57 less than unity. Despite these small uptake coefficients, significant partitioning into organic
17
18 58 semi-solids can occur, but trends in uptake do not necessarily follow those for partitioning. A
19
20 59 comprehensive understanding of the interactions of gases with the surface compared to the bulk
21
22 60 will help advance the current understanding of gas-particle interactions.
23
24
25
26

27 61
28
29

30 62
31
32

33 63
34
35

36 64
37
38

39 65
40
41

42 66
43
44

45 67
46
47

48 68
49
50

51 69
52
53

54 70
55
56
57
58
59
60

71 Introduction

72 Atmospheric aerosol particles are known to negatively impact air quality¹⁻⁴ and human health,⁵⁻¹⁴
73 as well as to affect climate.^{1, 2, 5, 15} Organic aerosols are major contributors, including both
74 primary emissions as well as secondary organic aerosol (SOA) particles formed in the oxidation
75 of volatile organic compounds (VOC). Particles with sufficient size (~100 nm) scatter light
76 significantly and act as cloud condensation nuclei, and their diameters strongly affect lung
77 deposition.¹⁶ However, mechanisms of nucleation and growth of organic particles to this size are
78 not yet understood well.¹⁷⁻²⁶

79 Particle growth has often been assumed to be governed by equilibrium partitioning
80 between the gas and particle phases.^{17, 19, 27-30} However, recent studies indicate that under some
81 conditions, SOA particles may be of relatively high viscosity and hence subject to diffusion
82 limitations and long equilibration timescales.³¹⁻⁴⁹ In this case, the mechanism may not be
83 governed by quasi-equilibrium growth,⁵⁰ but rather by a kinetically-controlled, diffusion limited
84 mechanism.⁵¹⁻⁵⁶ For example, Perraud *et al.*³⁹ showed that for particles formed by the oxidation
85 of α -pinene by ozone and NO₃ radical, the nitrate concentration in the particles was not
86 consistent with equilibrium partitioning between the gas and particle phases. Additionally,
87 Zaveri *et al.*⁵⁷ showed that both the growth and evaporation kinetics of bimodal SOA particles
88 were best reproduced by a semi-solid scenario. A recent study by Wang *et al.*⁵⁸ showed that the
89 dynamics of SOA formation and growth should take into account a number of processes that
90 occur simultaneously, rather than a quasi-equilibrium approach.

91 Slow diffusion throughout the particle due to a glassy or semi-solid phase state is
92 believed to limit the rate of uptake of incoming gas phase into the underlying layers of the
93 particle,⁴¹ and it is also expected to change the evaporation kinetics of molecules back into the

1
2
3 94 gas phase. For example, Vaden and co-workers³³ investigated the adsorption of insoluble
4
5 95 hydrophobic compounds including pyrene and dioctylphthalate (DOP) onto dry SOA generated
6
7
8 96 from the ozonolysis of α -pinene. Single particle measurements showed that these compounds
9
10 97 coated the SOA particle surface, forming either a solid nodule and aspherical particles (pyrene)
11
12 98 or layered particles (DOP). In both cases, the evaporation of underlying SOA was slowed down.
13
14
15 99 Effects of viscosity and diffusion were also observed in a number of recent studies involving
16
17 100 uptake onto organic aerosol and aerosol model systems or proxies using atmospherically relevant
18
19 101 gases including organics such as levoglucosan ($C_6H_{10}O_5$)⁵⁹ and polycyclic aromatic
20
21 102 hydrocarbons,⁶⁰⁻⁶² water (H_2O),^{49, 63-66} ozone (O_3),^{41, 67-70} hydroxyl radicals (OH),⁷⁰⁻⁷² nitrate
22
23 103 radicals (NO_3),⁷³ hydroperoxyl radicals (HO_2),⁷⁴ ammonia (NH_3)⁷⁵⁻⁷⁷ and amines.⁷⁸⁻⁸¹
24
25
26

27 104 A number of approaches have been developed to parameterize both physical and
28
29 105 chemical interactions of gases with atmospherically relevant particle systems.^{41, 68, 82-85} The
30
31 106 strength of the initial interaction of the gas with the surface must depend at a fundamental level
32
33
34 107 on both the structures and functional groups of the gas and the surface, and such properties must
35
36 108 ultimately provide the bedrock for model parameterizations. For example, to a first
37
38 109 approximation, it is expected that a polar gas with hydrogen-bonding potential would be taken up
39
40 110 on a polar surface with similar functional groups more readily than on a non-polar surface.
41
42
43

44 111 The interaction of a gas with a condensed phase where no reaction occurs involves a
45
46 112 number of individual steps:^{23, 86} (1) diffusion of the gas to the surface; (2) adsorption at the
47
48 113 surface; and (3) incorporation into the bulk via mass transport from the surface layer. The second
49
50 114 step is often referred to as surface accommodation and the third as bulk accommodation. The
51
52 115 efficiency of each step is generally expressed in terms of accommodation coefficients. The
53
54 116 surface accommodation coefficient (α_s) is the number of molecules adsorbed to the surface for
55
56
57
58
59
60

1
2
3 117 times longer than a single scattering event divided by the number of gas-surface collisions, while
4
5 118 the bulk accommodation coefficient (α_b) is the ratio of the number of molecules taken up into the
6
7
8 119 bulk to the number of gas-surface collisions. Experimentally, a net gas uptake coefficient (γ) is
9
10 120 usually measured, where γ is the ratio of the total number of molecules removed from the gas
11
12 121 phase (or the total number incorporated into the condensed phase) to the number of gas-surface
13
14
15 122 collisions. This net uptake coefficient reflects a combination of all of the processes above, and in
16
17 123 the case of reactive uptake, the chemistry as well.

19
20 124 In any event, there should be a range of uptake coefficients reflecting the gas-surface
21
22 125 attractive forces. It should be noted that the intermolecular forces between an incoming gas and
23
24 126 the surface of a particle may not be the same as those experienced by the gas when taken up into
25
26
27 127 the bulk. A comprehensive parameterization involving detailed gas-surface intermolecular
28
29 128 interactions remains challenging, in part due to the lack of available experimental data.

31
32 129 The goal of the present experiments was to probe the relationship between different gas-
33
34 130 surface interactions and net uptake coefficients as well as the bulk solubilities of the gas.
35
36
37 131 Organic nitrates are known to be formed by the OH radical oxidation of VOCs in the presence of
38
39 132 NO_x and are also known to be important products in NO_3 radical oxidation reactions.⁸⁷⁻⁹⁸ Alkyl
40
41 133 and multifunctional organic nitrates, including hydroxynitrates, have also been measured in both
42
43
44 134 ambient air and particles.⁹⁹⁻¹⁰⁵ Three different organic nitrates with varying functionalities,
45
46 135 structures, and vapor pressures, as well as various organic film substrates were studied. The
47
48 136 nitrates, shown in Figure 1, include two isomeric β -hydroxynitrate mixtures, β -hydroxypropyl
49
50 137 nitrate (HPN) and β -hydroxyhexyl nitrate (HHN), and 2-ethylhexyl nitrate (2EHN, an alkyl
51
52
53 138 nitrate). Organic nitrates are spectroscopically unique, exhibiting strong absorptions in the
54
55
56 139 infrared region (specific $-\text{ONO}_2$ stretches are at 850 cm^{-1} for the N-O stretch, 1280 cm^{-1} for the

1
2
3 140 symmetric NO₂ stretch, and 1630 cm⁻¹ for the asymmetric NO₂ stretch).^{90, 106} This facilitated
4
5 141 following uptake and desorption of the nitrates *in situ* and in real time using attenuated total
6
7 142 reflection Fourier transform infrared spectroscopy (ATR-FTIR). The substrates (Figure 1)
8
9
10 143 include a non-polar long chain alkane (triacontane, TC), an amorphous ester oligomer
11
12 144 (poly(ethylene adipate) di-hydroxy terminated, PEA), a keto-acid (pinonic acid, PA), and SOA
13
14
15 145 from α -pinene ozonolysis. The alkane might be considered a model for primary organic
16
17 146 aerosol,¹⁰⁷ while the keto-acid and ester are representative of functionalities found in SOA.¹⁰⁸⁻¹¹³
18
19 147 Both net initial uptake and partition coefficients were measured to provide insight into
20
21 148 interactions of gases with surfaces compared to the bulk, and desorption was also captured to
22
23 149 understand diffusivity back into the gas phase. Kinetic modeling and quantum chemical
24
25 150 calculations were applied to provide additional molecular level insight into these interactions.
26
27
28

29 151 **Experimental**

30 152 *Methods*

31
32
33
34
35 153 Figure 2 shows a schematic diagram of the ATR-FTIR cell. For each uptake experiment,
36
37 154 a Ge crystal coated with the target substrate was placed in the cell (total volume ~2 cm³) in the
38
39 155 sampling compartment of an FTIR spectrometer (Nicolet 6700). The spectrum of each sample
40
41 156 was acquired using 4 co-added scans with a resolution of 8 cm⁻¹, yielding a time resolution of 1
42
43 157 data point approximately every 3 seconds. The film alone was first exposed to 60 \pm 5 cm³ min⁻¹
44
45 158 clean, dry air from a purge air generator (Parker-Balston, model 75-62) for 15-300 seconds to
46
47 159 dry the film and to bring any spreading that might occur under a gas flow to a steady-state before
48
49 160 the addition of the nitrate. The organic nitrate was then introduced into the ATR cell by flowing
50
51 161 clean, dry air at a flow rate of 60 \pm 5 cm³ min⁻¹ over the pure liquid of each organic nitrate
52
53
54
55 162 contained in a glass trap at room temperature. The gas-phase concentrations were assumed to be
56
57
58
59
60

1
2
3 163 equivalent to the saturation vapor pressure of the organic nitrate. The trap was replenished daily
4
5 164 with fresh organic nitrate (synthesized hydroxynitrates were stored in a freezer under N₂ (g)). In
6
7
8 165 some cases, the organic nitrate signal in the IR decreased over the course of a day, indicating
9
10 166 there may have been some decomposition in the trap. When decomposition was observed, only
11
12 167 data from the first run of the day were used. Additional experiments where the time the film was
13
14
15 168 exposed to the organic nitrate was doubled also showed stability of the organic nitrate signal,
16
17 169 indicating decomposition was minimal over the length of the experiments.
18
19

20 170 The 2EHN was purchased and used as received. The HHN and HPN were synthesized by
21
22 171 scaling up the method of Cavdar and Saracoglu.¹¹⁴ In brief, epoxyhexane or epoxypropane were
23
24 172 reacted with bismuth (III) nitrate•5 H₂O in a 1:2 mole ratio (typical amounts were on the order of
25
26
27 173 10⁻² moles), in dichloromethane as the solvent. The reaction was carried out with constant
28
29 174 stirring for 16-24 hours at room temperature under N₂ (g), after which the solvent was
30
31 175 evaporated off *in vacuo* (Wheaton, SPIN-VAP). The liquid product was then purified using a
32
33
34 176 silica gel column, with a solvent system of 2:1 ethyl acetate:hexanes, and again the solvent was
35
36 177 removed using a roto-vap. As shown in the electronic supplementary information (ESI), the
37
38 178 resulting liquid product was characterized using FTIR (Nicolet 6700, Figure S1), GC-MS
39
40
41 179 (Agilent 7890a GC system with a 5975C MS detector, Figure S2), and ¹H NMR (Bruker
42
43 180 DRX500, 500 MHz, in CDCl₃ with 0.05% tetramethylsilane, Figure S3), with final purities of
44
45 181 ~87-90% for both HPN and HHN estimated from the NMR data. Impurities were identified as
46
47
48 182 residual solvent and the corresponding di-alcohol by comparison to pure standards.
49

50 183 In addition, the purity of the gas-phase organic hydroxynitrates (HHN and HPN) from the
51
52
53 184 headspace of the trap was examined by direct analysis in real-time mass spectrometry (DART-
54
55 185 MS) using a triple quadrupole mass spectrometer (Waters, Xevo TQ-S) with a DART ionization
56
57
58
59
60

1
2
3 186 source (Ion-Sense, DART SVP with Vapur® Interface). Since DART is an ambient ionization
4
5 187 method, quantification is difficult but identification of the nitrates and some impurities using this
6
7 188 method is reliable. Conditions used were the following: helium gas flow, 3.1 L min⁻¹; grid
8
9
10 189 electrode voltage, 350 V; DART temperature, 25 °C. DART-MS measurements were performed
11
12 190 at low temperature to minimize thermal decomposition of the organic nitrates.^{115, 116} All mass
13
14 191 spectra were recorded in the positive ion mode for m/z ranging from 25 to 400 amu. The mass
15
16 192 spectra for both HPN and HHN, as well as the mass spectra for the corresponding di-alcohols,
17
18 193 are shown in Figure S4. The predominant peaks in the DART spectra are due to $[2M+H-NO_2]^+$
19
20 194 at m/z 197 and 281 for HPN and HHN, respectively. There was little to no evidence for the
21
22 195 corresponding di-alcohol in the gas-phase above the liquid.
23
24
25

26 196 *FTIR Analysis*

27
28
29
30 197 These organic nitrates were chosen because of their range of vapor pressures, different
31
32 198 functional groups and unique spectral signatures in the IR. The characteristic peaks of the nitrate
33
34 199 were monitored over time (1280 and 1630 cm⁻¹) along with the carbonyl peaks of the organic
35
36 200 film (1700-1730 cm⁻¹) while the gas-phase nitrate flowed over the film. For TC, which has no
37
38 201 carbonyl functional group, the C-H peak at 2915 cm⁻¹ was followed. After the organic nitrate
39
40 202 signal reached equilibrium, the flow was replaced with 60 ± 5 cm³ min⁻¹ clean, dry air to follow
41
42 203 the desorption of the tracer as a function of time.
43
44
45

46 204 To quantify the amount of nitrate taken up into the film in units of molecules cm⁻², FTIR
47
48 205 cross-sections for the organic nitrate tracers (1280 cm⁻¹) and the organic substrates (-C=O stretch
49
50 206 at 1700-1730 cm⁻¹) were obtained using solution standards of known concentrations. Details on
51
52 207 the cross-section calculations are found in the ESI, and the cross sections for all compounds are
53
54
55
56
57
58
59
60

1
2
3 208 listed in Table S1. Pinonic acid gives a different signal in the solid phase (film) than in the liquid
4
5 209 (see Figure S5), and details on this quantification are given in the ESI.
6
7

8 210 To calculate the mole ratio of nitrate to carbonyl groups for each substrate, equation (1)
9
10 211 was used:
11
12

13
14 212
$$\frac{A_{\text{nit}}}{A_{\text{C=O}}} \times \frac{l_{\text{C=O}} \times \sigma_{\text{C=O}}}{l_{\text{nit}} \times \sigma_{\text{nit}}} = \frac{[-\text{ONO}_2]}{[\text{C=O}]} \quad (1)$$

15
16
17

18 213 In equation (1), A_{nit} and $A_{\text{C=O}}$ are the IR absorbances for the organic nitrate and the carbonyl of
19
20 214 the substrate, respectively, σ is the absorption cross-section ($\text{cm}^2 \text{mole}^{-1}$, base 10), and l is the
21
22 215 pathlength (cm) probed in the film at the selected wavenumbers for the carbonyl and the organic
23
24 216 nitrate. The concentrations of nitrate and substrate, $[-\text{ONO}_2]$ and $[\text{C=O}]$, are in moles $-\text{ONO}_2$
25
26 217 cm^{-3} and moles C=O cm^{-3} , respectively. The pathlength determination for the ATR beam is
27
28 218 described in the ESI, section 2. Substrate films were prepared to allow penetration of the IR
29
30 219 beam throughout the entire film if evenly spread over the crystal, but due to inhomogeneity in
31
32 220 the distribution of the films over the crystal surfaces (Figure S6), this may not be the case in
33
34 221 some regions of the film.
35
36
37
38

39 222 For uptake coefficients, the amount of nitrate taken up was determined from the organic
40
41 223 nitrate peak height using equation (2),
42
43

44 224
$$\frac{A_{\text{nit}}}{\sigma_{\text{nit}}} \times N_A = \{-\text{ONO}_2\} \quad (2)$$

45
46
47

48 225 where A is the absorbance of the organic nitrate, σ is the cross section of the organic nitrate in
49
50 226 $\text{cm}^2 \text{mole}^{-1}$ (base 10), N_A is Avogadro's number, and $\{-\text{ONO}_2\}$ is the amount of nitrate in the
51
52 227 film. Although expressed as as the number of $-\text{ONO}_2$ per cm^2 , it is the column integrated nitrate
53
54 228 and includes both surface and bulk contributions. By plotting the concentration over time as the
55
56
57
58
59
60

229 film is exposed to the organic nitrate and subsequently taking the initial slope of the initial data
 230 points ($t < 20$ s), the net uptake coefficient (γ) was quantified by equation (3):

$$231 \quad \gamma = \frac{R_0}{[\text{Gas}] \times \sqrt{\frac{RT}{2\pi M}}} \quad (3)$$

232 where R_0 is defined as the initial rate of uptake. Lastly, partition coefficients K were calculated
 233 using equation (4),

$$234 \quad K = \frac{[-\text{ONO}_2]_{\text{film}}}{[-\text{ONO}_2]_{\text{air}}} \quad (4)$$

235 where $[-\text{ONO}_2]_{\text{film}}$ and $[-\text{ONO}_2]_{\text{air}}$ are the concentrations of organic nitrate in the film and in air,
 236 respectively, in units of moles L^{-1} . The concentration in air was estimated using the saturation
 237 vapor pressure. The number of moles of $-\text{ONO}_2$ per L in the substrate film were calculated
 238 using equations (5), (6) and (7):

$$239 \quad \frac{\frac{A_{\text{nit}}}{I_{\text{nit}} \times \sigma_{\text{nit}}}}{\frac{A_{\text{C=O}}}{I_{\text{C=O}} \times \sigma_{\text{C=O}}} + \frac{A_{\text{nit}}}{I_{\text{nit}} \times \sigma_{\text{nit}}}} = \frac{[-\text{ONO}_2]}{[\text{C=O}] + [-\text{ONO}_2]} \quad (5)$$

$$240 \quad [\text{C=O}] \times \frac{n_{\text{sub}}}{n_{\text{C=O}}} = [\text{Sub}] \quad (6)$$

$$241 \quad \frac{[-\text{ONO}_2]}{[\text{Sub}] \times M_{\text{sub}}/\rho_{\text{sub}} + [-\text{ONO}_2] \times M_{\text{nit}}/\rho_{\text{nit}}} = [-\text{ONO}_2]_{\text{film}} \quad (7)$$

242 In equation (6), the $[\text{C=O}]$ (moles C=O cm^{-3}) is converted into $[\text{Sub}]$ (moles substrate cm^{-3})
 243 using the number of carbonyl groups on each substrate molecule (2 for PA, 12 for PEA, and
 244 assuming 2 for SOA).^{108, 109} In equation (7), moles of substrate and moles nitrate are converted
 245 to volume (in units of L) using the molecular weight (M , assuming 200 g mole^{-1} for SOA),¹⁰⁸⁻¹¹⁰
 246 and the densities in units of g L^{-1} (using $1.2 \times 10^3 \text{ g L}^{-1}$ for SOA).¹¹⁷

247 *Organic Film Preparation and Secondary Organic Aerosol Generation/Impaction*

248 Films were created by dissolving the pure solid in solvent (hexanes, dichloromethane,
249 methanol, or acetonitrile) and spreading a known volume (5-20 μL) of the solution onto the
250 exposed face of the ATR crystal. The solvent was removed using a flow of dry N_2 (g) until only
251 the dry solid remained.

252 SOA from the ozonolysis of α -pinene was generated in a large volume, slow flow,
253 stainless steel aerosol flow reactor described in detail elsewhere¹¹⁸ using initial concentrations of
254 250 ppb α -pinene and 250-350 ppb O_3 . The details on α -pinene SOA generation are presented in
255 the ESI and an example of the size distribution of the particles generated in the flow reactor is
256 shown in Figure S7. The polydisperse SOA particles formed in the flow reactor were collected
257 onto a Ge ATR crystal using a custom-designed impactor with a 50% cut-off diameter of 240
258 nm.³⁸ The particles were sampled at a total flow of 30 L min^{-1} for 10-20 minutes at the end of
259 the reactor corresponding to a reaction time of 31 minutes.

260 *Theoretical Calculations*

261 Relevant physical properties of these organic nitrates (molecular weight, vapor pressure,
262 and dipole moment) are given in Table 1. The dipole moment of each organic nitrate (including
263 both OH-terminated and nitrate-terminated isomers for HHN and HPN) was calculated as
264 described below. Their vapor pressures were estimated using two group contribution methods.¹¹⁹⁻
265 ¹²¹ The vapor pressures for 2EHN and HPN are on the border between VOC and intermediate
266 VOC (IVOC), while the lower vapor pressure of HHN classifies it as an IVOC.¹²² Note that for
267 HHN and HPN there are two isomers generated in the synthesis (hydroxy-terminated and nitrate-
268 terminated). Because these have different vapor pressures, the average of the two isomers was

1
2
3 269 used to calculate gas phase concentrations for the hydroxynitrates. While the predicted vapor
4
5 270 pressures differ slightly between the two methods, these differences are small and do not change
6
7
8 271 the general trends in the reported results.
9

10 272 Geometry optimization, frequency calculations, and dipole moments for the organic
11
12
13 273 nitrates were performed at the level of B3PW91^{123, 124} /aug-cc-pVDZ.¹²⁵ To test the adequacy of
14
15 274 the method for the dipole moments, isobutyl nitrate (IBN) was used as a test compound. The
16
17
18 275 dipole moment of IBN obtained here (3.7243D) is in excellent agreement with a previously
19
20 276 reported value (3.6806 D at the level of B3PW91/6-31G(d)),¹²⁶ and the values for the studied
21
22 277 organic nitrates also agree reasonably well with calculated dipole moments for other organic
23
24 278 nitrate species.¹²⁷ All calculations were performed using the Q-CHEM 4.3 program package.¹²⁸
25
26

27 279 The structures of the nitrate-PEA complexes were built using Packmol¹²⁹ software. These
28
29
30 280 structures were optimized using Gaussian09 (D 0.1) software¹³⁰ and the geometries were
31
32 281 confirmed as minima by the absence of imaginary frequencies. Counterpoise correction¹³¹ was
33
34 282 included to account for the Basis Set Superposition Error (BSSE) in binding energies nitrate-
35
36
37 283 PEA calculations. Density functional theory with the hybrid functional B3LYP^{132, 133} using the
38
39 284 6-31+G(d) Pople basis set,¹³⁴ and with Grimme's D3 correction for dispersion¹³⁵ were employed
40
41 285 for the energetics and structure calculations of the complex. This method has the capability to
42
43
44 286 describe both the electrostatic interactions due to the partial charges on the atoms and the very
45
46 287 significant dispersion interactions.
47
48

49 288 *KM-GAP Model*

50
51

52 289 The uptake of organic nitrates into the three different substrates was investigated using
53
54 290 the kinetic multi-layer model of gas-particle interactions in aerosols and clouds (KM-GAP).¹³⁶
55
56
57
58
59
60

1
2
3 291 This model is based on fundamental physical processes and explicitly treats the adsorption and
4
5 292 desorption of the organic nitrate to and from the surface of the substrate, partitioning of the
6
7 293 adsorbed organic nitrate into the bulk of the substrate, and bulk diffusion of the substrate and
8
9 294 nitrate. The bulk was treated with 100 layers which could each grow and shrink as molecules
10
11 295 diffused in and out of them, consequently the total thickness of the bulk increased and decreased
12
13 296 due to condensation and evaporation. The bulk diffusion coefficient of the nitrate ($D_{b,\text{nit}}$) and
14
15 297 substrate ($D_{b,\text{sub}}$) were treated to be composition-dependent using Vignes-type equations^{64, 67} as
16
17 298 described in the ESI, Section 4. The partition coefficients from the experiments were used as
18
19 299 fixed model inputs and the best fit film thicknesses were calculated from the model. The model-
20
21 300 predicted thicknesses are constrained to a small range of values based on the experimental data
22
23 301 provided. For PA and PEA, they are larger than those calculated assuming the substrate is
24
25 302 distributed equally over the entire surface of the crystal. This is reasonable since the solutions of
26
27 303 PA and PEA did not dry uniformly, with more material located in the center of the crystal (Fig.
28
29 304 S6). The model-predicted thickness for SOA is smaller than if spread equally. The impactor
30
31 305 deposits SOA unevenly,³⁸ being weighted towards the center (Fig. S6), and the amount
32
33 306 deposited to give sufficient carbonyl signals was about an order of magnitude greater than for
34
35 307 PEA and PA. The absolute number of nitrate molecules measured in the SOA may therefore
36
37 308 have been underestimated, which would lead to an underestimate of the model-predicted film
38
39 309 thickness. However, this does not change the conclusions.

310 *Reagents*

311 Reagents and sources were as follows: dodecane (Sigma Aldrich, $\geq 99\%$), methanol (EMD
312 Millipore, $\geq 99.9\%$), acetonitrile (EMD Millipore, $\geq 90\%$), epoxyhexane (Sigma-Aldrich, 97%),
313 epoxypropane (Sigma-Aldrich, $\geq 99\%$), bismuth (III) nitrate $\cdot 5 \text{ H}_2\text{O}$ (Sigma-Aldrich, 98%),

1
2
3 314 dichloromethane (EMD Millipore, $\geq 99.9\%$), chloroform-D (with 0.05% by volume
4
5 315 tetramethylsilane, Cambridge Isotope Laboratories Inc., 99.8%), (+)- α -pinene (Sigma-Aldrich,
6
7 316 $\geq 99\%$), hexanes (VWR Analytical, $>98.5\%$), dichloromethane (Macron, $\geq 99.5\%$), ethyl acetate
8
9
10 317 (EMD Chemical Inc., $>99.5\%$), triacontane (Sigma-Aldrich, 98%), L-(+)-tartaric acid (Sigma-
11
12 318 Aldrich, $\geq 99.5\%$), poly(ethylene adipate) di-hydroxy terminated (Sigma-Aldrich, average MW
13
14 319 1000), cis-pinonic acid (Sigma-Aldrich, 98%), 2-ethylhexyl nitrate (Sigma-Aldrich, 97%),
15
16 320 valeric acid (Sigma-Aldrich, $\geq 99\%$), 2-nonanone (Sigma-Aldrich, $\geq 99\%$), propanediol (Sigma-
17
18 321 Aldrich, $\geq 99.5\%$), hexanediol (Sigma-Aldrich, 98%), N₂ (Praxair, 99.999%), and O₂ (Praxair,
19
20 322 99.993%).
21
22
23

24 323 **Results and Discussion**

25 324 *ATR-FTIR Spectra.*

26
27 325 Figure 3a shows the ATR-FTIR spectra for the solid film substrates before exposure to
28
29 326 the organic nitrates, and Figure 3b shows typical spectra for each substrate after exposure to 5
30
31 327 ppm gaseous HHN. Similar spectra showing each substrate after exposure to 250 ppm HPN or
32
33 328 140 ppm 2EHN can be found in Figure S8. Note that the saturation vapor pressure of HHN is
34
35 329 much lower than that of HPN or 2EHN, limiting the HHN concentration that can be generated in
36
37 330 the gas phase. Despite the two orders of magnitude lower concentration, uptake of HHN is still
38
39 331 clearly evident onto SOA, PA and PEA. As seen in Figures 3 and S8, there was no observed
40
41 332 uptake onto TC, and uptake onto the Ge crystal itself was minimal for all three organic nitrates.
42
43
44
45
46
47
48

49 333 The lack of uptake of all the organic nitrates on TC is not surprising. With the absence of
50
51 334 polar interactions or hydrogen-bonding between the gas and the hydrocarbon surface, the
52
53 335 dispersion forces may simply be too weak to result in any significant uptake onto the TC (we use
54
55
56
57
58
59
60

1
2
3 336 here the terminology of "van der Waals' interactions" for all weak non-covalent forces, including
4
5 337 hydrogen-bonding, and use "dispersion interactions" specifically for forces due to induced
6
7 338 dipoles).¹³⁷ In contrast, there was significant uptake observed for the organic nitrates onto PA,
9
10 339 PEA and SOA.

11
12
13 340 Figure 4 shows typical data for the time-dependent uptake of the three organic nitrates on
14
15 341 SOA, PA and PEA respectively, calculated using equation (2) above. The curves are best fits
16
17 342 from the KM-GAP model,¹³⁶ discussed in detail below. In all cases, there is a rapid initial uptake
18
19 343 which then rises to a plateau, at which point there is no further net uptake. The concentrations of
20
21 344 the organic nitrates are significant, reaching as high as 3×10^{16} molecules cm^{-2} for HHN on PA.
22
23 345 The amount taken up is much larger than a monolayer ($\sim 10^{14}$ molecules cm^{-2}), which suggests
24
25 346 either a) that the organic nitrates adsorbed and created a film along the surface approximately
26
27 347 100 monolayers thick, or b) that the organic nitrates are not simply adsorbed onto the surface but
28
29 348 are penetrating and diffusing throughout the organic film. The former seems unlikely, and
30
31 349 diffusion through the organic films is feasible given the timescales of the experiments and
32
33 350 estimated thicknesses of the films. As discussed below, this is also supported by relatively slow
34
35 351 desorption of the nitrates out of the film.

352 *Net Uptake Coefficients*

353 From the initial rapid uptake, a net uptake coefficient γ can be obtained. These are
354 summarized in Table 2, and shown in Figure 5. In the framework proposed by Pöschl, Rudich
355 and Ammann⁸⁶ and Kolb *et al.*,²³ these would be equivalent to bulk accommodation coefficients
356 (α_b) because the nitrate in the entire film is interrogated by IR. In the application of the KM-

1
2
3 357 GAP model discussed below, the surface mass accommodation coefficients (α_s) were taken to be
4
5
6 358 one, and diffusion of the gas to the surface is not limiting under our conditions.
7

8
9 359 The limited number of data points in this initial time frame gives rise to significant error
10
11 360 bars, and may underestimate the rate of uptake as the films begin to take up the organic nitrate
12
13 361 and some re-evaporation from the film occurs. As discussed earlier, the gas-phase organic nitrate
14
15 362 concentrations may be overestimated and the substrate films may not be homogeneous in
16
17 363 thickness, which would also result in underestimates of the uptake coefficients. However, this
18
19 364 approach should provide reliable relative rates for the different organic nitrates and substrates, as
20
21 365 well as order-of-magnitude absolute values that can be used to provide insight into molecular
22
23 366 interactions between the gas and the surface films.
24
25
26

27
28 367 As seen in Figure 5, HHN has by far the largest net uptake coefficient for all three
29
30 368 substrates, with values over an order of magnitude higher than those of HPN and 2EHN. This is
31
32 369 not surprising as HHN has the largest capacity for intermolecular interactions, possessing both
33
34 370 the additional hydroxyl group for hydrogen bonding and the longer carbon backbone for
35
36 371 dispersion interactions. In sharp contrast, uptake of HHN is minimal on TC as well as on the
37
38 372 clean crystal (Fig. 3). Hence, hydrogen bonding and other van der Waals' forces with specific
39
40 373 functional groups on the substrates must play a significant role to anchor the incoming gas phase
41
42 374 molecule onto PA, PEA and SOA.
43
44
45

46
47 375 These measured uptake coefficients are orders of magnitude less than one. This is
48
49 376 reasonable given the range of previously reported uptake coefficients for both reactive and non-
50
51 377 reactive uptake. For an example of reactive uptake, Fairhurst *et al.*^{78, 79} reported that for the
52
53 378 uptake of various amines and ammonia with a series of dicarboxylic acids, net reactive uptake
54
55 379 coefficients ranged from 0.7 to less than 10^{-6} . Additionally, a previous study by Donaldson *et*

1
2
3 380 *al.*¹³⁸ showed that the unreactive uptake of certain gases onto organic films of oleic acid or
4
5 381 squalene ranged from $\sim 10^{-2}$ to less than 10^{-5} .
6
7

8 382 Calculations of the structures and binding energies for complexes of the nitrates with the
9
10 383 substrates can lend insight into the forces that provide the initial anchor for the incoming nitrate.
11
12 384 Binding energy calculations were carried out for complexes of one or two gas phase nitrate
13
14 385 molecules (2EHN, HPN and HHN) with one PEA substrate subunit. While PEA has an average
15
16 386 molecular weight of 1000 g mol^{-1} and thus contains 5-6 subunits, one PEA subunit was used to
17
18 387 represent the substrate due to computational constraints.
19
20
21
22

23 388 Figure 6 shows the optimized structures for one nitrate molecule interacting with one
24
25 389 PEA subunit for all the organic nitrates. The binding energies are summarized in Table S3. As
26
27 390 seen in Figure 6a, 2EHN is positioned horizontally over the PEA subunit where there are weaker
28
29 391 dispersion forces between its alkyl chain and that of PEA, whereas HPN forms one hydrogen
30
31 392 bond with the carbonyl group on the PEA (Fig. 6b). This is consistent with binding energies of
32
33 393 $11.8 \text{ kcal mol}^{-1}$ and $13.5 \text{ kcal mol}^{-1}$ for 2EHN and HPN, respectively. For HPN to be taken up,
34
35 394 the HPN molecule must find a carbonyl with which to form a hydrogen bond, which introduces a
36
37 395 steric component to the uptake. The interaction of 2EHN with the surface through dispersion
38
39 396 interactions is less sterically demanding. Thus, although the binding energy for 2EHN is
40
41 397 smaller, the higher net uptake coefficient for 2EHN is consistent with the lack of a significant
42
43 398 steric effect. Like HPN, HHN is also able to form a hydrogen bond with PEA to anchor it to the
44
45 399 substrate molecule (Fig. 6c) with a binding energy of $14.5 \text{ kcal mol}^{-1}$, and prefers to orient itself
46
47 400 vertically with the carbon tail away from the PEA.
48
49
50
51
52

53 401 Further insight was gained by carrying out calculations for two nitrate molecules
54
55 402 interacting with the PEA subunit. Figure S9 shows the optimized structures. The binding
56
57
58
59
60

1
2
3 403 energies for these structures are also found in Table S3. The binding energies for 2EHN and
4
5 404 HPN are similar (18.0 and 18.5 kcal mol⁻¹, respectively) and higher than for one organic nitrate
6
7 405 on one PEA subunit. The binding energy for two HHN molecules with one PEA subunit is much
8
9
10 406 higher, 30.0 kcal mol⁻¹. This is due to a contribution from hydrogen bonding between the HHN
11
12 407 nitrate functional group and the PEA terminal hydroxyl group. Since only one PEA subunit was
13
14 408 used to represent the substrate, and the polymer itself does not have repeating internal hydroxyl
15
16
17 409 groups, the importance of binding to the terminal hydroxyl and the binding energies may be
18
19 410 overestimated. However, the structure in Figure S9c shows both HHN molecules assemble
20
21 411 vertically, indicating the HHN molecules may be able to assemble along the surface of PEA
22
23 412 similar to a self-assembled monolayer, allowing for some dispersive interactions between the
24
25
26 413 HHN carbon backbones.

29 414 *Partition Coefficients and Mole Ratios of Organic Nitrates*

31
32 415 From the plateau region of Figure 4, mole ratios were calculated for each organic nitrate-
33
34 416 substrate combination. Table 3 shows the average ratio of moles of -ONO₂ to moles of C=O
35
36 417 after exposing SOA, PA and PEA to each organic nitrate for ~1000 seconds. The mole ratios
37
38 418 show large amounts of organic nitrate, up to 0.59 for the case of HHN on PA. These large ratios
39
40 419 of nitrate to substrate suggest that the nitrate is not simply adsorbing onto the surface of the solid
41
42 420 films, but is penetrating and diffusing into the films as discussed above.
43
44
45

46 421 Partition coefficients (K) were calculated as described above (equation 4) and are
47
48 422 summarized in Table 2 and Figure 7. As shown in Figure 7, HHN has the largest partition
49
50 423 coefficient (i.e., the largest solubility), with values up to two orders of magnitude larger than the
51
52 424 other organic nitrates. Additionally, the K values for HHN exhibit a clear trend across the
53
54
55
56
57
58
59
60

1
2
3 425 substrates, with $K^{PA} \sim K^{SOA} > K^{PEA}$. This same trend also holds for the K values of HPN, while
4
5 426 for 2EHN $K^{PA} > K^{SOA} \gtrsim K^{PEA}$.

7
8 427 While 2EHN and HPN both exhibit a decrease in partition coefficient from PA to PEA
9
10 428 and an increase from PEA to SOA, the relative magnitude of the partition coefficients changes.
11
12 429 For example, on PA $K^{2EHN} \gtrsim K^{HPN}$, but for SOA, $K^{2EHN} < K^{HPN}$. The differences in their
13
14 430 intermolecular interactions provide some insight into these trends. In the case of HPN, H-
15
16 431 bonding will dominate as it can both donate and accept H-bonds. In contrast, dispersion forces
17
18 432 will dominate for 2EHN with its larger alkyl chain. The crystal structure of PA exhibits a head-
19
20 433 to-tail arrangement, with the acidic hydrogen of one molecule hydrogen bonding to the ketone
21
22 434 carbonyl of the next molecule.¹³⁹ Although the PA in the film may no longer be in the
23
24 435 crystalline form, the FTIR spectrum for the PA film indicates the carbonyl-containing groups
25
26 436 are hydrogen-bonded (Figure S5), which is similar to the crystal structure. The acid carbonyl
27
28 437 does not participate in the self-hydrogen bonding network, and therefore can accept hydrogen
29
30 438 bonds from other molecules, for example from HPN. However, PA also has a significant
31
32 439 hydrocarbon backbone, allowing the dispersion forces to contribute as well. The relative
33
34 440 strength of these interactions are apparently similar enough to cause 2EHN and HPN to have
35
36 441 similar solubilities in PA.

37
38 442 For SOA, the partition coefficient for HPN is about a factor of two larger than for 2EHN,
39
40 443 indicating stronger attractive forces between the components of SOA and HPN. SOA is an
41
42 444 amorphous mixture containing many different acids and polar functionalities that are available to
43
44 445 hydrogen bond to the -OH group of HPN as well as its $-\text{ONO}_2$ group.¹⁰⁸ The additional
45
46 446 hydrogen-bonding capacity of HPN appears to play a significant role in enhancing its solubility
47
48 447 in SOA compared to the solubility of 2EHN.

1
2
3 448 It is important to note that vapor pressures are not necessarily a good measure of
4
5 449 incorporation of the nitrates into the organic substrates. Thus while 2EHN and HPN have similar
6
7 450 vapor pressures (Table 1), the solubility of HPN in SOA is double that of 2EHN. Similarly, the
8
9 451 net uptake coefficient of HPN on PEA is about a third of that for 2EHN.
10
11
12

13 452 Likewise, the O:C ratio (see ESI, section 3) is not a good predictor of uptake and
14
15 453 partitioning. The O:C ratios for PEA and SOA are similar, 0.52 and 0.50, respectively.
16
17 454 However the partition coefficients for all of the organic nitrates are greater on SOA than on PEA.
18
19 455 The O:C for PA is smaller (0.30), yet the partition coefficient of HHN is higher than in PEA and
20
21 456 perhaps SOA. Similarly, the solubility of 2EHN and HPN are relatively large for PA relative to
22
23 457 the PEA and SOA. Additionally, while the O:C ratio for PA is smaller than that of SOA and
24
25 458 PEA, the uptake coefficients are similar across all three substrates. This emphasizes the
26
27 459 importance of understanding intermolecular interactions both at the surface and in the bulk as
28
29 460 fundamental to the process of SOA growth in the atmosphere.
30
31
32
33

34 461 The relative values of the partition coefficients for 2EHN and HHN, which have similar
35
36 462 chain lengths but different functional groups, agrees well with air-octanol partition coefficients
37
38 463 for some organic nitrates reported by Treves *et al.*¹⁴⁰ The reported coefficients showed that the
39
40 464 addition of the hydroxyl group increased the solubility of the organic nitrates by over two orders
41
42 465 of magnitude when compared to a C₅ alkyl nitrate, which is attributed to the increased hydrogen
43
44 466 bonding capacity with the octanol. Additionally, when comparing different β -hydroxynitrates
45
46 467 (such as HHN and HPN), the solubility in octanol was also enhanced as the length of the carbon
47
48 468 chain increased.
49
50
51
52

53 469 *KM-GAP*
54
55
56
57
58
59
60

1
2
3 470 The KM-GAP model¹³⁶ was used to investigate diffusion of organic nitrates through the
4
5 471 organic film into the bulk. One observation is that bulk diffusion coefficients need to be treated
6
7 472 as composition-dependent with Vignes equations to reproduce the entire data set, and a
8
9 473 composition-independent constant diffusion coefficient scenario did not accurately capture the
10
11 474 data set. An example is shown in Figure 8 for uptake of HHN on PA. Although both
12
13 475 parameterizations fit the uptake of the organic nitrate onto the substrate reasonably well, a
14
15 476 constant diffusion coefficient over-predicted how quickly HHN would diffuse back out of the PA
16
17 477 film, whereas a composition-dependent diffusion coefficient was a better match to the
18
19 478 experimental data (Fig. 8, solid lines). The parameters and coefficients used for the constant
20
21 479 diffusion coefficient model are shown in Table S4.

22
23
24
25
26 480 Figure 9 shows the KM-GAP predicted concentration gradients for the organic nitrates as
27
28 481 a function of time. The y-axis of Figure 9 indicates the distance from the bottom of the film.
29
30 482 These profiles indicate that the organic nitrate has indeed penetrated through the entirety of the
31
32 483 film over the course of the experiments. Increases in the film thickness indicates that the organic
33
34 484 film has swelled due to uptake of significant amounts of the organic nitrate. Figure S10 shows
35
36 485 the accompanying changes in diffusion coefficients predicted by the KM-GAP model. The
37
38 486 profiles indicate that there is a plasticizing effect upon incorporation of the organic nitrate,
39
40 487 shown by the increases in diffusion coefficients for several nitrate-substrate systems.
41
42 488 Furthermore, upon desorption, the removal of the organic nitrate from the topmost layers of the
43
44 489 substrate results in decreasing diffusion coefficients in the upper layers of the film as they
45
46 490 partially re-solidify without the organic nitrate. This results in a ‘crusting’ scenario with higher
47
48 491 diffusion coefficients (and thus lower viscosities) in the lower layers of the film and a more
49
50 492 viscous outer layer or ‘crust’ towards the surface. Figure 10 shows an expanded view as an

1
2
3 493 example of the crusting on the surface of the film of SOA as 2EHN desorbs from the surface
4
5 494 layer. This ‘crusting’ effect has been observed in previous work by Boyd *et al.*¹⁴¹ on the
6
7
8 495 evaporation kinetics of mixed limonene and β -pinene SOA, as well as by Pfrang *et al.*¹⁴² on the
9
10 496 chemical aging and transformation of multi-component organic aerosol particles.

13 497 *Comparison of Trends in Uptake Coefficients and Partitioning*

16 498 HHN exhibits the largest partition and net uptake coefficients compared to the other
17
18 499 organic nitrates, and also provides the most pronounced differences in uptake versus solubility
19
20 500 across the three substrates. The uptake coefficient for HHN is similar for SOA, PA and PEA
21
22 501 (Fig. 5 and Table 2), while the solubility of HHN in PEA is lower than that in PA and SOA (Fig.
23
24 502 7 and Table 2). This suggests that the interactions between the nitrate and the substrate in the
25
26 503 bulk are different than those controlling uptake at the substrate surface.

30 504 Figure 11 compares the trends in net uptake and partition coefficients for the three
31
32 505 nitrates on SOA. While the uptake coefficient increases by a factor of 28 from 2EHN to HHN,
33
34 506 the partition coefficient increases by a factor of 88. Thus, the solubility increases relatively more
35
36 507 than the uptake coefficient, indicating that the relative contributions of the different attractive
37
38 508 forces between the organic nitrates and the substrate must differ for the surface relative to those
39
40 509 in the bulk. This is intuitively reasonable, given that the organic nitrates in the bulk are
41
42 510 surrounded by neighboring molecules with opportunities to optimize the full range of van der
43
44 511 Waals’ interactions, including H-bonding, electrostatic interactions between partial charges, and
45
46 512 dispersion interactions. On the other hand, an incoming gaseous organic nitrate molecule is
47
48 513 affected only by available functional groups located on the surface, which will determine the
49
50 514 nature and magnitude of the attractive forces. In the case of HHN on SOA, for example, if HHN
51
52 515 is H-bonded to the surface in such a manner that the interactions of the alkyl chain with the

1
2
3 516 surface are less than in the bulk where the HHN is engulfed by SOA components, relatively
4
5 517 smaller uptake coefficients than expected based on the bulk behavior could result. Consistent
6
7 518 with this, Figure 6c shows that HHN is predicted to be oriented perpendicular to the PEA
8
9 519 surface, minimizing dispersion forces between HHN and the surface PEA. This illustrates the
10
11 520 importance of understanding both the nature of the surface and the nature of the gas in predicting
12
13 521 uptake of gases into highly viscous particles, and hence their growth mechanisms in air.
14
15

16 17 522 **Conclusions**

18
19
20 523 Intermolecular interactions between gases and atmospheric particle surfaces play an
21
22 524 important role in SOA particle growth. The present results indicate that a combination of polar
23
24 525 and nonpolar interactions with the surface of SOA particles formed by the ozonolysis of α -
25
26 526 pinene play a role in gas uptake. However, the interactions determining this uptake are not
27
28 527 necessarily the same as those occurring in the bulk, and hence the uptake coefficients and
29
30 528 partition coefficients do not always correlate. Trends in vapor pressure are also not necessarily
31
32 529 good indicators of uptake or partitioning. Note that these uptake coefficients may be orders of
33
34 530 magnitude less than one and will certainly depend on both the nature of the gas and surface. Gas
35
36 531 partitioning into these substrates has the ability to change the viscosity of the film and thus to
37
38 532 increase the diffusion coefficients in the bulk. Furthermore, diffusion coefficients can decrease as
39
40 533 the nitrates diffuse back out due to the formation of a crust near the surface. This has
41
42 534 implications in the kinetics of condensed phase chemistry occurring in the bulk versus at the
43
44 535 surface of particles. More knowledge of the nature of the surface of SOA particles, and how
45
46 536 gaseous species interact with these surfaces, will allow for a better understanding of SOA
47
48 537 particle growth to better predict their effects on Earth's climate.
49
50
51
52
53
54

55 538 **Acknowledgements**

1
2
3 539 This work was funded by the NSF (Grant # 1647386), by the NSF Major Research
4
5 540 Instrumentation (MRI) program (Grants #1337080 and #0923323), and the Army Research
6
7 541 Office (Grant #W911NF1710105). M.S. acknowledges funding from NSF (CAREER, AGS-
8
9 542 1654104). The authors thank the University of California Irvine NMR Facility and Cambustion,
10
11 543 Ltd. (Cambridge, UK) for loan of the aerodynamic aerosol classifier.
12
13
14

15 544
16
17
18
19
20
21
22
23
24
25
26
27
28
29
30
31
32
33
34
35
36
37
38
39
40
41
42
43
44
45
46
47
48
49
50
51
52
53
54
55
56
57
58
59
60

545 **Table 1:** Molecular properties of the organic nitrates at 25 ° C.

546

Organic Nitrates	MW (g mol ⁻¹)	ρ (g mL ⁻¹)	Vapor Pressure using Moller ^{120, 121} (Pa)	Vapor Pressure ^d using SIMPOL.1 ¹¹⁹ (Pa)	Dipole Moment (D)
HHN	163	1.1	0.35 ^a	0.85	4.6220 ^a
			<u>0.65</u> ^b		2.8393 ^b
			Average ^c = 0.50 ± 0.21		
HPN	121	1.2	12 ^a	16	4.6191 ^a
			<u>35</u> ^b		4.7683 ^b
			Average ^c = 24 ± 16		
2EHN	175	0.96	14	18	3.9216

547 ^aHydroxy-terminated isomer

548 ^bNitrate-terminated isomer

549 ^cError bars are ±1 σ .

550 ^dSIMPOL.1 does not distinguish between isomers

551

552

553

554

555

556

557

558

559 **Table 2:** Average net uptake coefficients (γ) and partition coefficients (K).

Organic Nitrates	Substrates	Average Uptake Coefficient ^a (γ)	Average Partition Coefficient ^a (K)
HHN	SOA	$(2.5 \pm 0.2) \times 10^{-4}$	$(1.5 \pm 0.2) \times 10^7$
	PA	$(2.9 \pm 0.3) \times 10^{-4}$	$(1.8 \pm 0.2) \times 10^7$
	PEA	$(2.8 \pm 0.8) \times 10^{-4}$	$(7.3 \pm 1.8) \times 10^6$
HPN	SOA	$(1.0 \pm 0.3) \times 10^{-5}$	$(3.4 \pm 1.2) \times 10^5$
	PA	$(1.3 \pm 0.6) \times 10^{-5}$	$(2.4 \pm 0.7) \times 10^5$
	PEA	$(5.8 \pm 1.3) \times 10^{-6}$	$(9.5 \pm 3.5) \times 10^4$
2EHN	SOA	$(9.0 \pm 4.3) \times 10^{-6}$	$(1.7 \pm 0.1) \times 10^5$
	PA	$(3.2 \pm 1.6) \times 10^{-5}$	$(3.3 \pm 1.1) \times 10^5$
	PEA	$(1.8 \pm 0.3) \times 10^{-5}$	$(1.1 \pm 0.1) \times 10^5$

560 ^aError bars are statistical $\pm 1\sigma$ from the average of multiple experiments.

561

562

563

564

565

566

Table 3: Average mole ratios^a of $-\text{ONO}_2$ to $-\text{C}=\text{O}$ for PA, PEA, and SOA after exposure to each organic nitrate for 1047 seconds where equilibrium has been reached.

	Nitrates	Substrates	Mole Ratio ^a
		SOA	0.36 ± 0.06
	HHN	PA	0.59 ± 0.16
		PEA	0.12 ± 0.04
		SOA	0.55 ± 0.29
	HPN	PA	0.27 ± 0.12
		PEA	0.077 ± 0.031
		SOA	0.088 ± 0.007
	2EHN	PA	0.24 ± 0.12
		PEA	0.046 ± 0.006

^a Error bars are $\pm 1\sigma$ from the average of multiple experiments.

References

1. B. J. Finlayson-Pitts and J. N. Pitts, *Chemistry of the Upper and Lower Atmosphere: Theory, Experiments, and Applications*, Academic Press, 2000.
2. J. H. Seinfeld and S. N. Pandis, *Atmospheric Chemistry and Physics: From Air Pollution to Climate Change*, Wiley, 2006.
3. W. C. Hinds, *Aerosol Technology: Properties, Behavior, and Measurement of Airborne Particles*, John Wiley & Sons, 1982.
4. A. Singh, W. J. Bloss and F. D. Pope, 60 years of UK visibility measurements: impact of meteorology and atmospheric pollutants on visibility, *Atmos. Chem. Phys.*, 2017, **17**, 2085-2101.
5. U. Pöschl and M. Shiraiwa, Multiphase chemistry at the atmosphere–biosphere interface influencing climate and public health in the anthropocene, *Chem. Rev.*, 2015, **115**, 4440-4475.
6. C. A. Pope and D. W. Dockery, Health effects of fine particulate air pollution: lines that connect, *J. Air Waste Manage.*, 2006, **56**, 709-742.
7. J. L. Mauderly and J. C. Chow, Health effects of organic aerosols, *Inhal. Toxicol.*, 2008, **20**, 257-288.
8. M. R. Heal, P. Kumar and R. M. Harrison, Particles, air quality, policy and health, *Chem. Soc. Rev.*, 2012, **41**, 6606-6630.
9. A. Nel, Air pollution-related illness: effects of particles, *Science*, 2005, **308**, 804-806.
10. G. B. Hamra, N. Guha, A. Cohen, F. Laden, O. Raaschou-Nielsen, J. M. Samet, P. Vineis, F. Forastiere, P. Saldiva, T. Yorifuji and D. Loomis, Outdoor particulate matter exposure and lung cancer: a systematic review and meta-analysis, *Environ. Health Perspect.*, 2014, **122**, 906-911.
11. P. M. Mannucci, S. Harari, I. Martinelli and M. Franchini, Effects on health of air pollution: a narrative review, *Intern. Emerg. Med.*, 2015, **10**, 657-662.
12. R. E. Wyzga and A. C. Rohr, Long-term particulate matter exposure: attributing health effects to individual PM components, *J. Air Waste Manage.*, 2015, **65**, 523-543.
13. J. Lelieveld, J. S. Evans, M. Fnais, D. Giannadaki and A. Pozzer, The contribution of outdoor air pollution sources to premature mortality on a global scale, *Nature*, 2015, **525**, 367-374.
14. P. J. Landrigan, R. Fuller, N. J. R. Acosta, O. Adeyi, R. Arnold, N. Basu, A. B. Baldé, R. Bertollini, S. Bose-O'Reilly, J. I. Boufford, P. N. Breysse, T. Chiles, C. Mahidol, A. M. Coll-Seck, M. L. Cropper, J. Fobil, V. Fuster, M. Greenstone, A. Haines, D. Hanrahan, D. Hunter, M. Khare, A. Krupnick, B. Lanphear, B. Lohani, K. Martin, K. V. Mathiasen, M. A. McTeer, C. J. L. Murray, J. D. Ndahimananjara, F. Perera, J. Potočnik, A. S. Preker, J. Ramesh, J. Rockström, C. Salinas, L. D. Samson, K. Sandilya, P. D. Sly, K. R. Smith, A. Steiner, R. B. Stewart, W. A. Suk, O. C. P. van Schayck, G. N. Yadama, K. Yumkella and M. Zhong, The Lancet Commission on pollution and health, *The Lancet*, 2018, **391**, 462-512.
15. O. Boucher, D. Randall, P. Artaxo, C. Bretherton, G. Feingold, P. Forster, V.-M. Kerminen, Y. Kondo, H. Liao, U. and P. R. Lohmann, S.K. Satheesh, S. Sherwood, B. Stevens and X.Y. Zhang, 2013, Clouds and Aerosols, in *Climate Change 2013: The Physical Science Basis. Contribution of Working Group I to the Fifth Assessment Report of the Intergovernmental Panel on Climate Change*, eds. T. F. Stocker, D. Qin, G.-K.

- 1
2
3 632 Plattner, M. Tignor, S. K. Allen, J. Boschung, A. Nauels, Y. Xia, V. Bex and P. M.
4 633 Midgley, Cambridge University Press, Cambridge, United Kingdom and New York, NY,
5 634 USA, DOI: 10.1017/CBO9781107415324.
- 6
7 635 16. R. F. Phalen, *Inhalation studies: Foundation and techniques*, Informa Healthcare, 2009.
8 636 17. M. Kanakidou, J. H. Seinfeld, S. N. Pandis, I. Barnes, F. J. Dentener, M. C. Facchini, R.
9 637 Van Dingenen, B. Ervens, A. Nenes, C. J. Nielsen, E. Swietlicki, J. P. Putaud, Y.
10 638 Balkanski, S. Fuzzi, J. Horth, G. K. Moortgat, R. Winterhalter, C. E. L. Myhre, K.
11 639 Tsigaridis, E. Vignati, E. G. Stephanou and J. Wilson, Organic aerosol and global climate
12 640 modelling: a review, *Atmos. Chem. Phys.*, 2005, **5**, 1053-1123.
13 641 18. S. Fuzzi, M. O. Andreae, B. J. Huebert, M. Kulmala, T. C. Bond, M. Boy, S. J. Doherty,
14 642 A. Guenther, M. Kanakidou, K. Kawamura, V. M. Kerminen, U. Lohmann, L. M. Russell
15 643 and U. Pöschl, Critical assessment of the current state of scientific knowledge,
16 644 terminology, and research needs concerning the role of organic aerosols in the
17 645 atmosphere, climate, and global change, *Atmos. Chem. Phys.*, 2006, **6**, 2017-2038.
18 646 19. M. Hallquist, J. C. Wenger, U. Baltensperger, Y. Rudich, D. Simpson, M. Claeys, J.
19 647 Dommen, N. M. Donahue, C. George, A. H. Goldstein, J. F. Hamilton, H. Herrmann, T.
20 648 Hoffmann, Y. Iinuma, M. Jang, M. E. Jenkin, J. L. Jimenez, A. Kiendler-Scharr, W.
21 649 Maenhaut, G. McFiggans, T. F. Mentel, A. Monod, A. S. H. Prevot, J. H. Seinfeld, J. D.
22 650 Surratt, R. Szmigielski and J. Wildt, The formation, properties and impact of secondary
23 651 organic aerosol: current and emerging issues, *Atmos. Chem. Phys.*, 2009, **9**, 5155-5236.
24 652 20. J. P. D. Abbatt, A. K. Y. Lee and J. A. Thornton, Quantifying trace gas uptake to
25 653 tropospheric aerosol: recent advances and remaining challenges, *Chem. Soc. Rev.*, 2012,
26 654 **41**, 6555-6581.
27 655 21. R. Y. Zhang, G. H. Wang, S. Guo, M. L. Zarnora, Q. Ying, Y. Lin, W. G. Wang, M. Hu
28 656 and Y. Wang, Formation of urban fine particulate matter, *Chem. Rev.*, 2015, **115**, 3803-
29 657 3855.
30 658 22. R. Y. Zhang, A. Khalizov, L. Wang, M. Hu and W. Xu, Nucleation and growth of
31 659 nanoparticles in the atmosphere, *Chem. Rev.*, 2012, **112**, 1957-2011.
32 660 23. C. E. Kolb, R. A. Cox, J. P. D. Abbatt, M. Ammann, E. J. Davis, D. J. Donaldson, B. C.
33 661 Garrett, C. George, P. T. Griffiths, D. R. Hanson, M. Kulmala, G. McFiggans, U. Pöschl,
34 662 I. Riipinen, M. J. Rossi, Y. Rudich, P. E. Wagner, P. M. Winkler, D. R. Worsnop and C.
35 663 D. O' Dowd, An overview of current issues in the uptake of atmospheric trace gases by
36 664 aerosols and clouds, *Atmos. Chem. Phys.*, 2010, **10**, 10561-10605.
37 665 24. I. Riipinen, T. Yli-Juuti, J. R. Pierce, T. Petäjä, D. R. Worsnop, M. Kulmala and N. M.
38 666 Donahue, The contribution of organics to atmospheric nanoparticle growth, *Nat. Geosci.*,
39 667 2012, **5**, 453.
40 668 25. M. Shrivastava, C. D. Cappa, J. Fan, A. H. Goldstein, A. B. Guenther, J. L. Jimenez, C.
41 669 Kuang, A. Laskin, S. T. Martin, N. L. Ng, T. Petäjä, J. R. Pierce, P. J. Rasch, P. Roldin, J.
42 670 H. Seinfeld, J. Shilling, J. N. Smith, J. A. Thornton, R. Volkamer, J. Wang, D. R.
43 671 Worsnop, R. A. Zaveri, A. Zelenyuk and Q. Zhang, Recent advances in understanding
44 672 secondary organic aerosol: implications for global climate forcing, *Rev. Geophys.*, 2017,
45 673 **55**, 509-559.
46 674 26. D. Stolzenburg, L. Fischer, A. L. Vogel, M. Heinritzi, M. Schervish, M. Simon, A. C.
47 675 Wagner, L. Dada, L. R. Ahonen, A. Amorim, A. Baccarini, P. S. Bauer, B. Baumgartner,
48 676 A. Bergen, F. Bianchi, M. Breitenlechner, S. Brilke, S. Buenrostro Mazon, D. Chen, A.
49 677 Dias, D. C. Draper, J. Duplissy, I. El Haddad, H. Finkenzeller, C. Frege, C. Fuchs, O.

- 1
2
3 678 Garmash, H. Gordon, X. He, J. Helm, V. Hofbauer, C. R. Hoyle, C. Kim, J. Kirkby, J.
4 679 Kontkanen, A. Kürten, J. Lampilahti, M. Lawler, K. Lehtipalo, M. Leiminger, H. Mai, S.
5 680 Mathot, B. Mentler, U. Molteni, W. Nie, T. Nieminen, J. B. Nowak, A. Ojdanic, A.
6 681 Onnela, M. Passananti, T. Petäjä, L. L. J. Quéléver, M. P. Rissanen, N. Sarnela, S.
7 682 Schallhart, C. Tauber, A. Tomé, R. Wagner, M. Wang, L. Weitz, D. Wimmer, M. Xiao,
8 683 C. Yan, P. Ye, Q. Zha, U. Baltensperger, J. Curtius, J. Dommen, R. C. Flagan, M.
9 684 Kulmala, J. N. Smith, D. R. Worsnop, A. Hansel, N. M. Donahue and P. M. Winkler,
10 685 Rapid growth of organic aerosol nanoparticles over a wide tropospheric temperature
11 686 range, *Proc. Natl. Acad. Sci. U.S.A.*, 2018, DOI: 10.1073/pnas.1807604115.
12
13 687 27. J. F. Pankow, Further discussion of the octanol/air partition coefficient K_{OA} as a
14 688 correlating parameter for gas/particle partitioning coefficients, *Atmos. Environ.*, 1998, **32**,
15 689 1493-1497.
16
17 690 28. J. F. Pankow, An absorption model of gas/particle partitioning of organic compounds in
18 691 the atmosphere, *Atmos. Environ.*, 1994, **28**, 185-188.
19 692 29. N. M. Donahue, I. K. Ortega, W. Chuang, I. Riipinen, F. Riccobono, S. Schobesberger, J.
20 693 Dommen, U. Baltensperger, M. Kulmala, D. R. Worsnop and H. Vehkamäki, How do
21 694 organic vapors contribute to new-particle formation?, *Faraday Discuss.*, 2013, **165**, 91-
22 695 104.
23
24 696 30. N. M. Donahue, A. L. Robinson, C. O. Stanier and S. N. Pandis, Coupled partitioning,
25 697 dilution, and chemical aging of semivolatile organics, *Environ. Sci. Technol.*, 2006, **40**,
26 698 2635-2643.
27 699 31. M. Shiraiwa and J. H. Seinfeld, Equilibration timescale of atmospheric secondary organic
28 700 aerosol partitioning, *Geophys. Res. Lett.*, 2012, **39**, L24801,
29 701 DOI:24810.21029/22012gl054008.
30
31 702 32. J. P. Reid, A. K. Bertram, D. O. Topping, A. Laskin, S. T. Martin, M. D. Petters, F. D.
32 703 Pope and G. Rovelli, The viscosity of atmospherically relevant organic particles, *Nat.*
33 704 *Commun.*, 2018, **9**, 956, DOI: 10.1038/s41467-41018-03027-z.
34 705 33. T. D. Vaden, D. Imre, J. Beránek, M. Shrivastava and A. Zelenyuk, Evaporation kinetics
35 706 and phase of laboratory and ambient secondary organic aerosol, *Proc. Natl. Acad. Sci.*
36 707 *U.S.A.*, 2011, **108**, 2190-2195.
37
38 708 34. A. Virtanen, J. Kannosto, H. Kuuluvainen, A. Arffman, J. Joutsensaari, E. Saukko, L.
39 709 Hao, P. Yli-Pirila, P. Tiitta, J. K. Holopainen, J. Keskinen, D. R. Worsnop, J. N. Smith
40 710 and A. Laaksonen, Bounce behavior of freshly nucleated biogenic secondary organic
41 711 aerosol particles, *Atmos. Chem. Phys.*, 2011, **11**, 8759-8766.
42 712 35. L. Renbaum-Wolff, J. W. Grayson, A. P. Bateman, M. Kuwata, M. Sellier, B. J. Murray,
43 713 J. E. Shilling, S. T. Martin and A. K. Bertram, Viscosity of alpha-pinene secondary
44 714 organic material and implications for particle growth and reactivity, *Proc. Natl. Acad.*
45 715 *Sci. U.S.A.*, 2013, **110**, 8014-8019.
46
47 716 36. T. Koop, J. Bookhold, M. Shiraiwa and U. Pöschl, Glass transition and phase state of
48 717 organic compounds: dependency on molecular properties and implications for secondary
49 718 organic aerosols in the atmosphere, *Phys. Chem. Chem. Phys.*, 2011, **13**, 19238-19255.
50 719 37. S. M. Zhou, M. Shiraiwa, R. D. McWhinney, U. Pöschl and J. P. D. Abbatt, Kinetic
51 720 limitations in gas-particle reactions arising from slow diffusion in secondary organic
52 721 aerosol, *Faraday Discuss.*, 2013, **165**, 391-406.
53
54
55
56
57
58
59
60

- 1
2
3 722 38. C. Kidd, V. Perraud, L. M. Wingen and B. J. Finlayson-Pitts, Integrating phase and
4 723 composition of secondary organic aerosol from the ozonolysis of alpha-pinene, *Proc.*
5 724 *Natl. Acad. Sci. U.S.A.*, 2014, **111**, 7552-7557.
- 6 725 39. V. Perraud, E. A. Bruns, M. J. Ezell, S. N. Johnson, Y. Yu, M. L. Alexander, A.
7 726 Zelenyuk, D. Imre, W. L. Chang, D. Dabdub, J. F. Pankow and B. J. Finlayson-Pitts,
8 727 Nonequilibrium atmospheric secondary organic aerosol formation and growth, *Proc.*
9 728 *Natl. Acad. Sci. U.S.A.*, 2012, **109**, 2836-2841.
- 10 729 40. A. Virtanen, J. Joutsensaari, T. Koop, J. Kannosto, P. Yli-Pirila, J. Leskinen, J. M.
11 730 Makela, J. K. Holopainen, U. Pöschl, M. Kulmala, D. R. Worsnop and A. Laaksonen, An
12 731 amorphous solid state of biogenic secondary organic aerosol particles, *Nature*, 2010, **467**,
13 732 824-827.
- 14 733 41. M. Shiraiwa, M. Ammann, T. Koop and U. Pöschl, Gas uptake and chemical aging of
15 734 semisolid organic aerosol particles, *Proc. Natl. Acad. Sci. U.S.A.*, 2011, **108**, 11003-
16 735 11008.
- 17 736 42. C. D. Cappa and K. R. Wilson, Evolution of organic aerosol mass spectra upon heating:
18 737 implications for OA phase and partitioning behavior, *Atmos. Chem. Phys.*, 2011, **11**,
19 738 1895-1911.
- 20 739 43. P. J. Ziemann, Phase matters for aerosols, *Nature*, 2010, **467**, 797-798.
- 21 740 44. F. H. Marshall, R. E. H. Miles, Y. C. Song, P. B. Ohm, R. M. Power, J. P. Reid and C. S.
22 741 Dutcher, Diffusion and reactivity in ultraviscous aerosol and the correlation with particle
23 742 viscosity, *Chem. Sci.*, 2016, **7**, 1298-1308.
- 24 743 45. N. A. Hosny, C. Fitzgerald, C. Tong, M. Kalberer, M. K. Kuimova and F. D. Pope,
25 744 Fluorescent lifetime imaging of atmospheric aerosols: a direct probe of aerosol viscosity,
26 745 *Faraday Discuss.*, 2013, **165**, 343-356.
- 27 746 46. N. A. Hosny, C. Fitzgerald, A. Vyšniauskas, A. Athanasiadis, T. Berkemeier, N. Uygur,
28 747 U. Pöschl, M. Shiraiwa, M. Kalberer, F. D. Pope and M. K. Kuimova, Direct imaging of
29 748 changes in aerosol particle viscosity upon hydration and chemical aging, *Chem. Sci.*,
30 749 2016, **7**, 1357-1367.
- 31 750 47. Y. Zhang, M. S. Sanchez, C. Douet, Y. Wang, A. P. Bateman, Z. Gong, M. Kuwata, L.
32 751 Renbaum-Wolff, B. B. Sato, P. F. Liu, A. K. Bertram, F. M. Geiger and S. T. Martin,
33 752 Changing shapes and implied viscosities of suspended submicron particles, *Atmos. Chem.*
34 753 *Phys.*, 2015, **15**, 79819-77829.
- 35 754 48. A. Pajunoja, J. Malila, L. Hao, J. Joutsensaari, K. E. J. Lehtinen and A. Virtanen,
36 755 Estimating the viscosity range of SOA particles based on their coalescence time, *Aerosol*
37 756 *Sci. Technol.*, 2014, **48**, i-iv.
- 38 757 49. A. Pajunoja, A. T. Lambe, J. Hakala, N. Rastak, M. J. Cummings, J. F. Brogan, L. Hao,
39 758 M. Paramonov, J. Hong, N. L. Prisle, J. Malila, S. Romakkaniemi, K. E. J. Lehtinen, A.
40 759 Laaksonen, M. Kulmala, P. Massoli, T. B. Onasch, N. M. Donahue, I. Riipinen, P.
41 760 Davidovits, D. R. Worsnop, T. Petäjä and A. Virtanen, Adsorptive uptake of water by
42 761 semisolid secondary organic aerosols, *Geophys. Res. Lett.*, 2015, **42**, 3063-3068.
- 43 762 50. H. Mai, M. Shiraiwa, R. C. Flagan and J. H. Seinfeld, Under what conditions can
44 763 equilibrium gas-particle partitioning be expected to hold in the atmosphere?, *Environ.*
45 764 *Sci. Technol.*, 2015, **49**, 11485-11491.
- 46 765 51. L. I. Kleinman, S. R. Springston, J. Wang, P. H. Daum, Y. N. Lee, L. J. Nunnermacker,
47 766 G. I. Senum, J. Weinstein-Lloyd, M. L. Alexander, J. Hubbe, J. Ortega, R. A. Zaveri, M.

- 1
2
3 767 R. Canagaratna and J. Jayne, The time evolution of aerosol size distribution over the
4 768 Mexico City plateau, *Atmos. Chem. Phys.*, 2009, **9**, 4261-4278.
- 5 769 52. F. Yu, A secondary organic aerosol formation model considering successive oxidation
6 770 aging and kinetic condensation of organic compounds: global scale implications, *Atmos.*
7 771 *Chem. Phys.*, 2011, **11**, 1083-1099.
- 8 772 53. K. Dzepina, R. M. Volkamer, S. Madronich, P. Tulet, I. M. Ulbrich, Q. Zhang, C. D.
9 773 Cappa, P. J. Ziemann and J. L. Jimenez, Evaluation of recently-proposed secondary
10 774 organic aerosol models for a case study in Mexico City, *Atmos. Chem. Phys.*, 2009, **9**,
11 775 5681-5709.
- 12 776 54. C. D. Cappa and J. L. Jimenez, Quantitative estimates of the volatility of ambient organic
13 777 aerosol, *Atmos. Chem. Phys.*, 2010, **10**, 5409-5424.
- 14 778 55. X. Zhang, S. N. Pandis and J. H. Seinfeld, Diffusion-limited versus quasi-equilibrium
15 779 aerosol growth, *Aerosol Sci. Technol.*, 2012, **46**, 874-885.
- 16 780 56. M. Shiraiwa, Y. Li, A. P. Tsimpidi, V. A. Karydis, T. Berkemeier, S. N. Pandis, J.
17 781 Lelieveld, T. Koop and U. Pöschl, Global distribution of particle phase state in
18 782 atmospheric secondary organic aerosols, *Nat. Commun.*, 2017, **8**, 15002, DOI:
19 783 15010.11038/ncomms15002.
- 20 784 57. R. A. Zaveri, J. E. Shilling, A. Zelenyuk, J. Liu, D. M. Bell, E. L. D'Ambro, C. J. Gaston,
21 785 J. A. Thornton, A. Laskin, P. Lin, J. Wilson, R. C. Easter, J. Wang, A. K. Bertram, S. T.
22 786 Martin, J. H. Seinfeld and D. R. Worsnop, Growth kinetics and size distribution
23 787 dynamics of viscous secondary organic aerosol, *Environ. Sci. Technol.*, 2018, **52**, 1191-
24 788 1199.
- 25 789 58. C. Wang, F. Wania and K.-U. Goss, Is secondary organic aerosol yield governed by
26 790 kinetic factors rather than equilibrium partitioning?, *Environ. Sci. Process. Impact*, 2018,
27 791 **20**, 245-252.
- 28 792 59. Z. Gong, Y. Han, P. Liu, J. Ye, F. N. Keutsch, K. A. McKinney and S. T. Martin,
29 793 Influence of particle physical state on the uptake of medium-sized organic molecules,
30 794 *Environ. Sci. Technol.*, 2018, **52**, 8381-8389.
- 31 795 60. A. Zelenyuk, D. G. Imre, J. Wilson, D. M. Bell, K. J. Suski, M. Shrivastava, J. Beránek,
32 796 M. L. Alexander, A. L. Kramer and S. L. Massey Simonich, The effect of gas-phase
33 797 polycyclic aromatic hydrocarbons on the formation and properties of biogenic secondary
34 798 organic aerosol particles, *Faraday Discuss.*, 2017, **200**, 143-164.
- 35 799 61. A. Zelenyuk, D. Imre, J. Beránek, E. Abramson, J. Wilson and M. Shrivastava, Synergy
36 800 between secondary organic aerosols and long-range transport of polycyclic aromatic
37 801 hydrocarbons, *Environ. Sci. Technol.*, 2012, **46**, 12459-12466.
- 38 802 62. E. Abramson, D. Imre, J. Beránek, J. Wilson and A. Zelenyuk, Experimental
39 803 determination of chemical diffusion within secondary organic aerosol particles, *Phys.*
40 804 *Chem. Chem. Phys.*, 2013, **15**, 2983-2991.
- 41 805 63. B. Zobrist, V. Soonsin, B. P. Luo, U. K. Krieger, C. Marcolli, T. Peter and T. Koop,
42 806 Ultra-slow water diffusion in aqueous sucrose glasses, *Phys. Chem. Chem. Phys.*, 2011,
43 807 **13**, 3514-3526.
- 44 808 64. D. M. Lienhard, A. J. Huisman, U. K. Krieger, Y. Rudich, C. Marcolli, B. Luo, D. L.
45 809 Bones, J. P. Reid, A. T. Lambe and M. R. Canagaratna, Viscous organic aerosol particles
46 810 in the upper troposphere: diffusivity-controlled water uptake and ice nucleation?, *Atmos.*
47 811 *Chem. Phys.*, 2015, **15**, 13599-13613.

- 1
2
3 812 65. H. J. Tong, J. P. Reid, D. L. Bones, B. P. Luo and U. K. Krieger, Measurements of the
4 813 timescales for the mass transfer of water in glassy aerosol at low relative humidity and
5 814 ambient temperature, *Atmos. Chem. Phys.*, 2011, **11**, 4739-4754.
- 6 815 66. D. L. Bones, J. P. Reid, D. M. Lienhard and U. K. Krieger, Comparing the mechanism of
7 816 water condensation and evaporation in glassy aerosol, *Proc. Natl. Acad. Sci. U.S.A.*,
8 817 2012, **109**, 11613-11618.
- 9 818 67. T. Berkemeier, S. S. Steimer, U. K. Krieger, T. Peter, U. Pöschl, M. Ammann and M.
10 819 Shiraiwa, Ozone uptake on glassy, semi-solid and liquid organic matter and the role of
11 820 reactive oxygen intermediates in atmospheric aerosol chemistry, *Phys. Chem. Chem.*
12 821 *Phys.*, 2016, **18**, 12662-12674.
- 13 822 68. S. Zhou, M. Shiraiwa, R. D. McWhinney, U. Pöschl and J. P. D. Abbatt, Kinetic
14 823 limitations in gas-particle reactions arising from slow diffusion in secondary organic
15 824 aerosol, *Faraday Discuss.*, 2013, **165**, 391-406.
- 16 825 69. N. O. A. Kwamena, M. G. Staikova, D. J. Donaldson, I. J. George and J. P. D. Abbatt,
17 826 Role of the aerosol substrate in the heterogeneous ozonation reactions of surface-bound
18 827 PAHs, *J. Phys. Chem. A*, 2007, **111**, 11050-11058.
- 19 828 70. L. Lee and K. Wilson, The reactive-diffusive length of OH and ozone in model organic
20 829 aerosols, *J. Phys. Chem. A*, 2016, **120**, 6800-6812.
- 21 830 71. J. H. Slade and D. A. Knopf, Multiphase OH oxidation kinetics of organic aerosol: the
22 831 role of particle phase state and relative humidity, *Geophys. Res. Lett.*, 2014, **41**, 5297-
23 832 5306.
- 24 833 72. A. M. Arangio, J. H. Slade, T. Berkemeier, U. Pöschl, D. A. Knopf and M. Shiraiwa,
25 834 Multiphase chemical kinetics of OH radical uptake by molecular organic markers of
26 835 biomass burning aerosols: humidity and temperature dependence, surface reaction, and
27 836 bulk diffusion, *J. Phys. Chem. A*, 2015, **119**, 4533-4544.
- 28 837 73. M. Shiraiwa, U. Pöschl and D. A. Knopf, Multiphase chemical kinetics of NO₃ radicals
29 838 reacting with organic aerosol components from biomass burning, *Environ. Sci. Technol.*,
30 839 2012, **46**, 6630-6636.
- 31 840 74. P. S. J. Lakey, T. Berkemeier, M. Krapf, J. Dommen, S. S. Steimer, L. K. Whalley, T.
32 841 Ingham, M. T. Baeza-Romero, U. Pöschl, M. Shiraiwa, M. Ammann and D. E. Heard,
33 842 The effect of viscosity and diffusion on the HO₂ uptake by sucrose and secondary organic
34 843 aerosol particles, *Atmos. Chem. Phys.*, 2016, **16**, 13035-13047.
- 35 844 75. M. Kuwata and S. T. Martin, Phase of atmospheric secondary organic material affects its
36 845 reactivity, *Proc. Natl. Acad. Sci. U.S.A.*, 2012, **109**, 17354-17359.
- 37 846 76. D. M. Bell, D. Imre, S. T. Martin and A. Zelenyuk, The properties and behavior of α -
38 847 pinene secondary organic aerosol particles exposed to ammonia under dry conditions,
39 848 *Phys. Chem. Chem. Phys.*, 2017, **19**, 6497-6507.
- 40 849 77. Y. J. Li, P. Liu, Z. Gong, Y. Wang, A. P. Bateman, C. Bergoend, A. K. Bertram and S. T.
41 850 Martin, Chemical reactivity and liquid/nonliquid states of secondary organic material,
42 851 *Environ. Sci. Technol.*, 2015, **49**, 13264-13274.
- 43 852 78. M. C. Fairhurst, M. J. Ezell, C. Kidd, P. S. J. Lakey, M. Shiraiwa and B. J. Finlayson-
44 853 Pitts, Kinetics, mechanisms and ionic liquids in the uptake of n-butylamine onto low
45 854 molecular weight dicarboxylic acids, *Phys. Chem. Chem. Phys.*, 2017, **19**, 4827-4839.
- 46 855 79. M. C. Fairhurst, M. J. Ezell and B. J. Finlayson-Pitts, Knudsen cell studies of the uptake
47 856 of gaseous ammonia and amines onto C₃-C₇ solid dicarboxylic acids, *Phys. Chem. Chem.*
48 857 *Phys.*, 2017, **19**, 26296-26309.

- 1
2
3 858 80. X. Gao, Y. Zhang and Y. Liu, A kinetics study of the heterogeneous reaction of n-
4 859 butylamine with succinic acid using an ATR-FTIR flow reactor, *Phys. Chem. Chem.*
5 860 *Phys.*, 2018, **20**, 15464-15472.
- 6 861 81. L. P. Chan and C. K. Chan, Role of the aerosol phase state in ammonia/amines exchange
7 862 reactions, *Environ. Sci. Technol.*, 2013, **47**, 5755-5762.
- 8 863 82. T. Berkemeier, A. J. Huisman, M. Ammann, M. Shiraiwa, T. Koop and U. Pöschl,
9 864 Kinetic regimes and limiting cases of gas uptake and heterogeneous reactions in
10 865 atmospheric aerosols and clouds: a general classification scheme, *Atmos. Chem. Phys.*,
11 866 2013, **13**, 6663-6686.
- 12 867 83. M. Ammann, U. Pöschl and Y. Rudich, Effects of reversible adsorption and Langmuir-
13 868 Hinshelwood surface reactions on gas uptake by atmospheric particles, *Phys. Chem.*
14 869 *Chem. Phys.*, 2003, **5**, 351-356.
- 15 870 84. M. Shiraiwa, C. Pfrang and U. Pöschl, Kinetic multi-layer model of aerosol surface and
16 871 bulk chemistry (KM-SUB): the influence of interfacial transport and bulk diffusion on the
17 872 oxidation of oleic acid by ozone, *Atmos. Chem. Phys.*, 2010, **10**, 3673-3691.
- 18 873 85. P. Roldin, A. C. Eriksson, E. Z. Nordin, E. Hermansson, D. Mogensen, A. Rusanen, M.
19 874 Boy, E. Swietlicki, B. Svenningsson, A. Zelenyuk and J. Pagels, Modelling non-
20 875 equilibrium secondary organic aerosol formation and evaporation with the aerosol
21 876 dynamics, gas- and particle-phase chemistry kinetic multilayer model ADCHAM, *Atmos.*
22 877 *Chem. Phys.*, 2014, **14**, 7953-7993.
- 23 878 86. U. Pöschl, Y. Rudich and M. Ammann, Kinetic model framework for aerosol and cloud
24 879 surface chemistry and gas-particle interactions - Part 1: General equations, parameters,
25 880 and terminology, *Atmos. Chem. Phys.*, 2007, **7**, 5989-6023.
- 26 881 87. A. Matsunaga and P. J. Ziemann, Yields of β -hydroxynitrates and dihydroxynitrates in
27 882 aerosol formed from OH radical-initiated reactions of linear alkenes in the presence of
28 883 NO_x , *J. Phys. Chem. A*, 2009, **113**, 599-606.
- 29 884 88. N. Sobanski, J. Thieser, J. Schuladen, C. Sauvage, W. Song, J. Williams, J. Lelieveld and
30 885 J. N. Crowley, Day and night-time formation of organic nitrates at a forested mountain
31 886 site in south-west Germany, *Atmos. Chem. Phys.*, 2017, **17**, 4115-4130.
- 32 887 89. R. Atkinson, S. M. Aschmann, W. P. Carter, A. M. Winer and J. N. Pitts Jr, Alkyl nitrate
33 888 formation from the nitrogen oxide (NO_x)-air photooxidations of C_2 - C_8 n-alkanes, *J. Phys.*
34 889 *Chem.*, 1982, **86**, 4563-4569.
- 35 890 90. J. M. Roberts, The atmospheric chemistry of organic nitrates, *Atmos. Environ. Part A*,
36 891 1990, **24**, 243-287.
- 37 892 91. J. L. Fry, A. Kiendler-Scharr, A. W. Rollins, T. Brauers, S. S. Brown, H. P. Dorn, W. P.
38 893 Dubé, H. Fuchs, A. Mensah, F. Rohrer, R. Tillmann, A. Wahner, P. J. Wooldridge and R.
39 894 C. Cohen, SOA from limonene: role of NO_3 in its generation and degradation, *Atmos.*
40 895 *Chem. Phys.*, 2011, **11**, 3879-3894.
- 41 896 92. M. Spittler, I. Barnes, I. Bejan, K. Brockmann, T. Benter and K. Wirtz, Reactions of NO_3
42 897 radicals with limonene and α -pinene: product and SOA formation, *Atmos. Environ.*,
43 898 2006, **40**, 116-127.
- 44 899 93. E. A. Bruns, V. Perraud, A. Zelenyuk, M. J. Ezell, S. N. Johnson, Y. Yu, D. Imre, B. J.
45 900 Finlayson-Pitts and M. L. Alexander, Comparison of FTIR and particle mass
46 901 spectrometry for the measurement of particulate organic nitrates, *Environ. Sci. Technol.*,
47 902 2010, **44**, 1056-1061.

- 1
2
3 903 94. R. Atkinson and J. Arey, Atmospheric degradation of volatile organic compounds, *Chem.*
4 904 *Rev.*, 2003, **103**, 4605-4638.
- 5 905 95. J. L. Fry, D. C. Draper, K. C. Barsanti, J. N. Smith, J. Ortega, P. M. Winkler, M. J.
6 906 Lawler, S. S. Brown, P. M. Edwards, R. C. Cohen and L. Lee, Secondary organic aerosol
7 907 formation and organic nitrate yield from NO₃ oxidation of biogenic hydrocarbons,
8 908 *Environ. Sci. Technol.*, 2014, **48**, 11944-11953.
- 9 909 96. N. L. Ng, S. S. Brown, A. T. Archibald, E. Atlas, R. C. Cohen, J. N. Crowley, D. A. Day,
10 910 N. M. Donahue, J. L. Fry, H. Fuchs, R. J. Griffin, M. I. Guzman, H. Herrmann, A.
11 911 Hodzic, Y. Iinuma, J. L. Jimenez, A. Kiendler-Scharr, B. H. Lee, D. J. Luecken, J. Mao,
12 912 R. McLaren, A. Mutzel, H. D. Osthoff, B. Ouyang, B. Picquet-Varrault, U. Platt, H. O. T.
13 913 Pye, Y. Rudich, R. H. Schwantes, M. Shiraiwa, J. Stutz, J. A. Thornton, A. Tilgner, B. J.
14 914 Williams and R. A. Zaveri, Nitrate radicals and biogenic volatile organic compounds:
15 915 oxidation, mechanisms, and organic aerosol, *Atmos. Chem. Phys.*, 2017, **17**, 2103-2162.
- 16 916 97. J. H. Slade, C. de Perre, L. Lee and P. B. Shepson, Nitrate radical oxidation of γ -
17 917 terpinene: hydroxy nitrate, total organic nitrate, and secondary organic aerosol yields,
18 918 *Atmos. Chem. Phys.*, 2017, **17**, 8635-8650.
- 19 919 98. C. Espada, J. Grossenbacher, K. Ford, T. Couch and P. B. Shepson, The production of
20 920 organic nitrates from various anthropogenic volatile organic compounds, *Int. J. Chem.*
21 921 *Kinet.*, 2005, **37**, 675-685.
- 22 922 99. A. W. Rollins, S. Pusede, P. Wooldridge, K. E. Min, D. R. Gentner, A. H. Goldstein, S.
23 923 Liu, D. A. Day, L. M. Russell, C. L. Rubitschun, J. D. Surratt and R. C. Cohen,
24 924 Gas/particle partitioning of total alkyl nitrates observed with TD-LIF in Bakersfield, *J.*
25 925 *Geophys. Res. Atmos.*, 2013, **118**, 6651-6662.
- 26 926 100. J. Kastler and K. Ballschmiter, Bifunctional alkyl nitrates – trace constituents of the
27 927 atmosphere, *Fresenius J. Anal. Chem.*, 1998, **360**, 812-816.
- 28 928 101. B. H. Lee, C. Mohr, F. D. Lopez-Hilfiker, A. Lutz, M. Hallquist, L. Lee, P. Romer, R. C.
29 929 Cohen, S. Iyer, T. Kurten, W. W. Hu, D. A. Day, P. Campuzano-Jost, J. L. Jimenez, L.
30 930 Xu, N. L. Ng, H. Y. Guo, R. J. Weber, R. J. Wild, S. S. Brown, A. Koss, J. de Gouw, K.
31 931 Olson, A. H. Goldstein, R. Seco, S. Kim, K. McAvey, P. B. Shepson, T. Starn, K.
32 932 Baumann, E. S. Edgerton, J. M. Liu, J. E. Shilling, D. O. Miller, W. Brune, S.
33 933 Schobesberger, E. L. D'Ambro and J. A. Thornton, Highly functionalized organic nitrates
34 934 in the southeast United States: contribution to secondary organic aerosol and reactive
35 935 nitrogen budgets, *Proc. Natl. Acad. Sci. U.S.A.*, 2016, **113**, 1516-1521.
- 36 936 102. J. M. O'Brien, P. B. Shepson, K. Muthuramu, C. Hao, H. Niki, D. R. Hastie, R. Taylor
37 937 and P. B. Roussel, Measurements of alkyl and multifunctional organic nitrates at a rural
38 938 site in Ontario, *J. Geophys. Res. Atmos.*, 1995, **100**, 22795-22804.
- 39 939 103. J. M. O'Brien, P. B. Shepson, Q. Wu, T. Biesenthal, J. W. Bottenheim, H. A. Wiebe, K.
40 940 G. Anlauf and P. Brickell, Production and distribution of organic nitrates, and their
41 941 relationship to carbonyl compounds in an urban environment, *Atmos. Environ.*, 1997, **31**,
42 942 2059-2069.
- 43 943 104. C. Zuth, A. L. Vogel, S. Okenfeld, R. Huesmann and T. Hoffmann, Ultra-high-resolution
44 944 mass spectrometry in real-time: atmospheric pressure chemical ionization orbitrap mass
45 945 spectrometry (ApCI-Orbitrap-MS) of atmospheric organic aerosol, *Anal. Chem.*, 2018,
46 946 DOI: 10.1021/acs.analchem.8b00671, DOI: 10.1021/acs.analchem.1028b00671.

- 1
2
3 947 105. A. E. Perring, S. E. Pusede and R. C. Cohen, An observational perspective on the
4 948 atmospheric impacts of alkyl and multifunctional nitrates on ozone and secondary
5 949 organic aerosol, *Chem. Rev.*, 2013, **113**, 5848-5870.
- 6 950 106. G. Socrates, *Infrared and Raman Characteristic Group Frequencies*, John Wiley & Sons,
7 951 New York, 2001.
- 8 952 107. Q. Zhang, D. R. Worsnop, M. R. Canagaratna and J. L. Jimenez, Hydrocarbon-like and
9 953 oxygenated organic aerosols in Pittsburgh: insights into sources and processes of organic
10 954 aerosols, *Atmos. Chem. Phys.*, 2005, **5**, 3289-3311.
- 11 955 108. X. Zhang, R. C. Mcvay, D. D. Huang, N. F. Dalleska, B. Aumont, R. C. Flagan and J. H.
12 956 Seinfeld, Formation and evolution of molecular products in alpha-pinene secondary
13 957 organic aerosol, *Proc. Natl. Acad. Sci. U.S.A.*, 2015, **112**, 14168-14173.
- 14 958 109. R. Winterhalter, R. Van Dingenen, B. R. Larsen, N. R. Jensen and J. Hjorth, LC-MS
15 959 analysis of aerosol particles from the oxidation of α -pinene by ozone and OH-radicals,
16 960 *Atmos. Chem. Phys. Discuss.*, 2003, **2003**, 1-39.
- 17 961 110. B. Witkowski and T. Gierczak, Early stage composition of SOA produced by α -
18 962 pinene/ozone reaction: α -acyloxyhydroperoxy aldehydes and acidic dimers, *Atmos.*
19 963 *Environ.*, 2014, **95**, 59-70.
- 20 964 111. K. Kristensen, T. Cui, H. Zhang, A. Gold, M. Glasius and J. D. Surratt, Dimers in α -
21 965 pinene secondary organic aerosol: effect of hydroxyl radical, ozone, relative humidity
22 966 and aerosol acidity, *Atmos. Chem. Phys.*, 2014, **14**, 4201-4218.
- 23 967 112. K. Kristensen, Å. K. Watne, J. Hammes, A. Lutz, T. Petäjä, M. Hallquist, M. Bilde and
24 968 M. Glasius, High-molecular weight dimer esters are major products in aerosols from α -
25 969 pinene ozonolysis and the boreal forest, *Environ. Sci. Technol. Lett.*, 2016, **3**, 280-285.
- 26 970 113. K. S. Docherty, W. Wu, Y. B. Lim and P. J. Ziemann, Contributions of organic peroxides
27 971 to secondary aerosol formed from reactions of monoterpenes with O₃, *Environ. Sci.*
28 972 *Technol.*, 2005, **39**, 4049-4059.
- 29 973 114. H. Cavdar and N. Saracoglu, Synthesis of new β -hydroxy nitrate esters as potential
30 974 glycomimetics or vasodilators, *Eur. J. Org. Chem.*, 2008, **2008**, 4615-4621.
- 31 975 115. B. Holger, S. Friedrich and S. Wolfram, Thermal decomposition of 2-ethylhexyl nitrate
32 976 (2-EHN), *Int. J. Chem. Kinet.*, 2002, **34**, 34-38.
- 33 977 116. D. A. Day, P. J. Wooldridge, M. B. Dillon, J. A. Thornton and R. C. Cohen, A thermal
34 978 dissociation laser-induced fluorescence instrument for in situ detection of NO₂, peroxy
35 979 nitrates, alkyl nitrates, and HNO₃, *J. Geophys. Res. Atmos.*, 2002, **107**, DOI:
36 980 10.1029/2001jd000779.
- 37 981 117. A. Zelenyuk, J. Yang, C. Song, R. A. Zaveri and D. Imre, A new real-time method for
38 982 determining particles' sphericity and density: application to secondary organic aerosol
39 983 formed by ozonolysis of α -pinene, *Environ. Sci. Technol.*, 2008, **42**, 8033-8038.
- 40 984 118. M. J. Ezell, S. N. Johnson, Y. Yu, V. Perraud, E. A. Bruns, M. L. Alexander, A.
41 985 Zelenyuk, D. Dabdub and B. J. Finlayson-Pitts, A new aerosol flow system for
42 986 photochemical and thermal studies of tropospheric aerosols, *Aerosol Sci. Technol.*, 2010,
43 987 **44**, 329-338.
- 44 988 119. J. F. Pankow and W. E. Asher, SIMPOL.1: a simple group contribution method for
45 989 predicting vapor pressures and enthalpies of vaporization of multifunctional organic
46 990 compounds, *Atmos. Chem. Phys.*, 2008, **8**, 2773-2796.

- 1
2
3 991 120. B. Moller, J. Rarey and D. Ramjugernath, Estimation of the vapour pressure of non-
4 992 electrolyte organic compounds via group contributions and group interactions, *J. Mol.*
5 993 *Liq.*, 2008, **143**, 52-63.
- 6 994 121. Y. Nannoolal, J. Rarey, D. Ramjugernath and W. Cordes, Estimation of pure component
7 995 properties: Part 1. Estimation of the normal boiling point of non-electrolyte organic
8 996 compounds via group contributions and group interactions, *Fluid Phase Equilib.*, 2004,
9 997 **226**, 45-63.
- 10 998 122. N. M. Donahue, W. Chuang, S. A. Epstein, J. H. Kroll, D. R. Worsnop, A. L. Robinson,
11 999 P. J. Adams and S. N. Pandis, Why do organic aerosols exist? Understanding aerosol
12 1000 lifetimes using the two-dimensional volatility basis set, *Environ. Chem.*, 2013, **10**, 151-
13 1001 157.
- 14 1002 123. A. D. Becke, A new mixing of Hartree–Fock and local density-functional theories, *J.*
15 1003 *Chem. Phys.*, 1993, **98**, 1372-1377.
- 16 1004 124. J. P. Perdew, K. Burke and Y. Wang, Generalized gradient approximation for the
17 1005 exchange-correlation hole of a many-electron system, *Phys. Rev. B*, 1996, **54**, 16533.
- 18 1006 125. T. H. Dunning Jr, Gaussian basis sets for use in correlated molecular calculations. I. The
19 1007 atoms boron through neon and hydrogen, *J. Chem. Phys.*, 1989, **90**, 1007-1023.
- 20 1008 126. J. S.-Y. Yu, α -Pinene organic nitrate synthesis, formation, and simulation, *Thesis*
21 1009 *Manuscript*, 2010.
- 22 1010 127. A. L. Lockwood, P. B. Shepson, M. N. Fiddler and M. Alaghmand, Isoprene nitrates:
23 1011 preparation, separation, identification, yields, and atmospheric chemistry, *Atmos. Chem.*
24 1012 *Phys.*, 2010, **10**, 6169-6178.
- 25 1013 128. Y. Shao, Z. Gan, E. Epifanovsky, A. T. B. Gilbert, M. Wormit, J. Kussmann, A. W.
26 1014 Lange, A. Behn, J. Deng, X. Feng, D. Ghosh, M. Goldey, P. R. Horn, L. D. Jacobson, I.
27 1015 Kaliman, R. Z. Khaliullin, T. Kuś, A. Landau, J. Liu, E. I. Proynov, Y. M. Rhee, R. M.
28 1016 Richard, M. A. Rohrdanz, R. P. Steele, E. J. Sundstrom, H. L. Woodcock, P. M.
29 1017 Zimmerman, D. Zuev, B. Albrecht, E. Alguire, B. Austin, G. J. O. Beran, Y. A. Bernard,
30 1018 E. Berquist, K. Brandhorst, K. B. Bravaya, S. T. Brown, D. Casanova, C.-M. Chang, Y.
31 1019 Chen, S. H. Chien, K. D. Closser, D. L. Crittenden, M. Diedenhofen, R. A. DiStasio, H.
32 1020 Do, A. D. Dutoi, R. G. Edgar, S. Fatehi, L. Fusti-Molnar, A. Ghysels, A. Golubeva-
33 1021 Zadorozhnaya, J. Gomes, M. W. D. Hanson-Heine, P. H. P. Harbach, A. W. Hauser, E.
34 1022 G. Hohenstein, Z. C. Holden, T.-C. Jagau, H. Ji, B. Kaduk, K. Khistyayev, J. Kim, J. Kim,
35 1023 R. A. King, P. Klunzinger, D. Kosenkov, T. Kowalczyk, C. M. Krauter, K. U. Lao, A. D.
36 1024 Laurent, K. V. Lawler, S. V. Levchenko, C. Y. Lin, F. Liu, E. Livshits, R. C. Lochan, A.
37 1025 Luenser, P. Manohar, S. F. Manzer, S.-P. Mao, N. Mardirossian, A. V. Marenich, S. A.
38 1026 Maurer, N. J. Mayhall, E. Neuscammann, C. M. Oana, R. Olivares-Amaya, D. P. O'Neill,
39 1027 J. A. Parkhill, T. M. Perrine, R. Peverati, A. Prociuk, D. R. Rehn, E. Rosta, N. J. Russ, S.
40 1028 M. Sharada, S. Sharma, D. W. Small, A. Sodt, T. Stein, D. Stück, Y.-C. Su, A. J. W.
41 1029 Thom, T. Tsuchimochi, V. Vanovschi, L. Vogt, O. Vydrov, T. Wang, M. A. Watson, J.
42 1030 Wenzel, A. White, C. F. Williams, J. Yang, S. Yeganeh, S. R. Yost, Z.-Q. You, I. Y.
43 1031 Zhang, X. Zhang, Y. Zhao, B. R. Brooks, G. K. L. Chan, D. M. Chipman, C. J. Cramer,
44 1032 W. A. Goddard, M. S. Gordon, W. J. Hehre, A. Klamt, H. F. Schaefer, M. W. Schmidt,
45 1033 C. D. Sherrill, D. G. Truhlar, A. Warshel, X. Xu, A. Aspuru-Guzik, R. Baer, A. T. Bell,
46 1034 N. A. Besley, J.-D. Chai, A. Dreuw, B. D. Dunietz, T. R. Furlani, S. R. Gwaltney, C.-P.
47 1035 Hsu, Y. Jung, J. Kong, D. S. Lambrecht, W. Liang, C. Ochsenfeld, V. A. Rassolov, L. V.
48 1036 Slipchenko, J. E. Subotnik, T. Van Voorhis, J. M. Herbert, A. I. Krylov, P. M. W. Gill

- 1
2
3 1037 and M. Head-Gordon, Advances in molecular quantum chemistry contained in the Q-
4 1038 Chem 4 program package, *Mol. Phys.*, 2015, **113**, 184-215.
- 5 1039 129. L. Martínez, R. Andrade, E. G. Birgin and J. M. Martínez, PACKMOL: A package for
6 1040 building initial configurations for molecular dynamics simulations, *J. Comput. Chem.*,
7 1041 2009, **30**, 2157-2164.
- 8 1042 130. M. J. Frisch, G. W. Trucks, H. B. Schlegel, G. E. Scuseria, M. A. Robb, J. R. Cheeseman,
9 1043 G. Scalmani, V. Barone, G. A. Petersson, H. Nakatsuji, X. Li, M. Caricato, A. Marenich,
10 1044 J. Bloino, B. G. Janesko, R. Gomperts, B. Mennucci, H. P. Hratchian, J. V. Ortiz, A. F.
11 1045 Izmaylov, J. L. Sonnenberg, D. Williams-Young, F. Ding, F. Lipparini, F. Egidi, J.
12 1046 Goings, B. Peng, A. Petrone, T. Henderson, D. Ranasinghe, V. G. Zakrzewski, J. Gao, N.
13 1047 Rega, G. Zheng, W. Liang, M. Hada, M. Ehara, K. Toyota, R. Fukuda, J. Hasegawa, M.
14 1048 Ishida, T. Nakajima, Y. Honda, O. Kitao, H. Nakai, T. Vreven, K. Throssell, J. A.
15 1049 Montgomery Jr., J. E. Peralta, F. Ogliaro, M. Bearpark, J. J. Heyd, E. Brothers, K. N.
16 1050 Kudin, V. N. Staroverov, T. Keith, R. Kobayashi, J. Normand, K. Raghavachari, A.
17 1051 Rendell, J. C. Burant, S. S. Iyengar, J. Tomasi, M. Cossi, J. M. Millam, M. Klene, C.
18 1052 Adamo, R. Cammi, J. W. Ochterski, R. L. Martin, K. Morokuma, O. Farkas, J. B.
19 1053 Foresman and D. J. Fox, Gaussian 09, Revision A.02, *Gaussian 09, Revision A.02*, 2009.
- 20 1054 131. F. B. van Duijneveldt, J. G. C. M. van Duijneveldt-van de Rijdt and J. H. van Lenthe,
21 1055 State of the art in counterpoise theory, *Chem. Rev.*, 1994, **94**, 1873-1885.
- 22 1056 132. A. D. Becke, Density-functional thermochemistry. III. The role of exact exchange, *J.*
23 1057 *Chem. Phys.*, 1993, **98**, 5648-5652.
- 24 1058 133. P. Stephens, F. Devlin, C. Chabalowski and M. J. Frisch, Ab initio calculation of
25 1059 vibrational absorption and circular dichroism spectra using density functional force
26 1060 fields, *J. Phys. Chem.*, 1994, **98**, 11623-11627.
- 27 1061 134. R. Ditchfield, W. J. Hehre and J. A. Pople, Self-consistent molecular-orbital methods. IX.
28 1062 An extended gaussian-type basis for molecular-orbital studies of organic molecules, *J.*
29 1063 *Chem. Phys.*, 1971, **54**, 724-728.
- 30 1064 135. S. Grimme, J. Antony, S. Ehrlich and H. Krieg, A consistent and accurate ab initio
31 1065 parametrization of density functional dispersion correction (DFT-D) for the 94 elements
32 1066 H-Pu, *J. Chem. Phys.*, 2010, **132**, 154104.
- 33 1067 136. M. Shiraiwa, C. Pfrang, T. Koop and U. Pöschl, Kinetic multi-layer model of gas-particle
34 1068 interactions in aerosols and clouds (KM-GAP): linking condensation, evaporation and
35 1069 chemical reactions of organics, oxidants and water, *Atmos. Chem. Phys.*, 2012, **12**, 2777-
36 1070 2794.
- 37 1071 137. J. Israelachvili, *Intermolecular & Surface Forces*, Academic Press, Second edn., 1991.
- 38 1072 138. D. J. Donaldson, B. T. Mmereki, S. R. Chaudhuri, S. Handley and M. Oh, Uptake and
39 1073 reaction of atmospheric organic vapours on organic films, *Faraday Discuss.*, 2005, **130**,
40 1074 227-239.
- 41 1075 139. P. A. Vanderhoff, H. W. Thompson and R. A. Lalancette, Structure of (\pm)-cis-pinonic
42 1076 acid, *Acta. Cryst. C*, 1986, **42**, 1766-1769.
- 43 1077 140. K. Treves, L. Shragina and Y. Rudich, Measurement of octanol-air partition coefficients
44 1078 using solid-phase microextraction (SPME)—application to hydroxy alkyl nitrates, *Atmos.*
45 1079 *Environ.*, 2001, **35**, 5843-5854.
- 46 1080 141. C. M. Boyd, T. Nah, L. Xu, T. Berkemeier and N. L. Ng, Secondary organic aerosol
47 1081 (SOA) from nitrate radical oxidation of monoterpenes: effects of temperature, dilution,

- 1
2
3 1082 and humidity on aerosol formation, mixing, and evaporation, *Environ. Sci. Technol.*,
4 1083 2017, **51**, 7831-7841.
5 1084 142. C. Pfrang, M. Shiraiwa and U. Pöschl, Chemical ageing and transformation of diffusivity
6 1085 in semi-solid multi-component organic aerosol particles, *Atmos. Chem. Phys.*, 2011, **11**,
7 1086 7343-7354.
8 1087
9 1087
10 1088
11
12
13
14
15
16
17
18
19
20
21
22
23
24
25
26
27
28
29
30
31
32
33
34
35
36
37
38
39
40
41
42
43
44
45
46
47
48
49
50
51
52
53
54
55
56
57
58
59
60

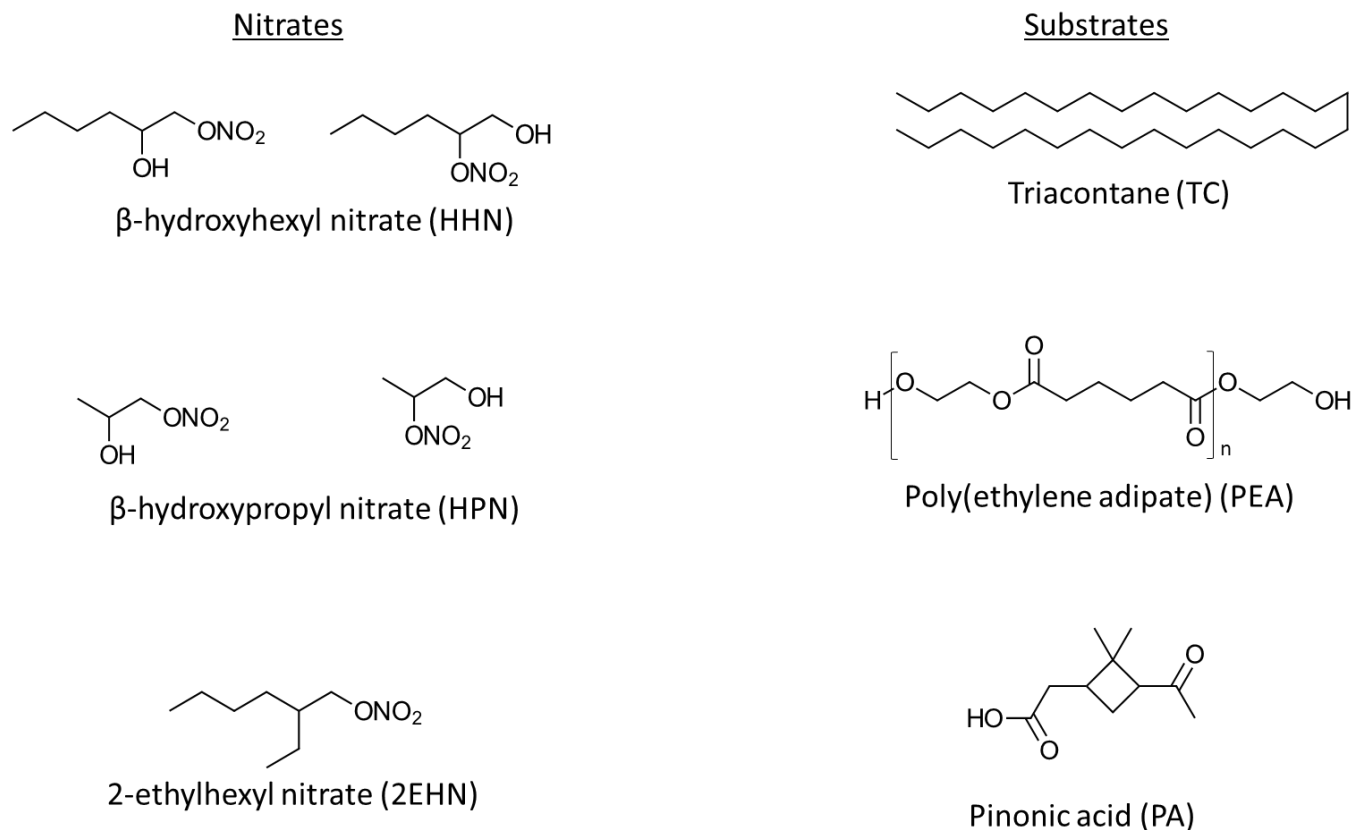
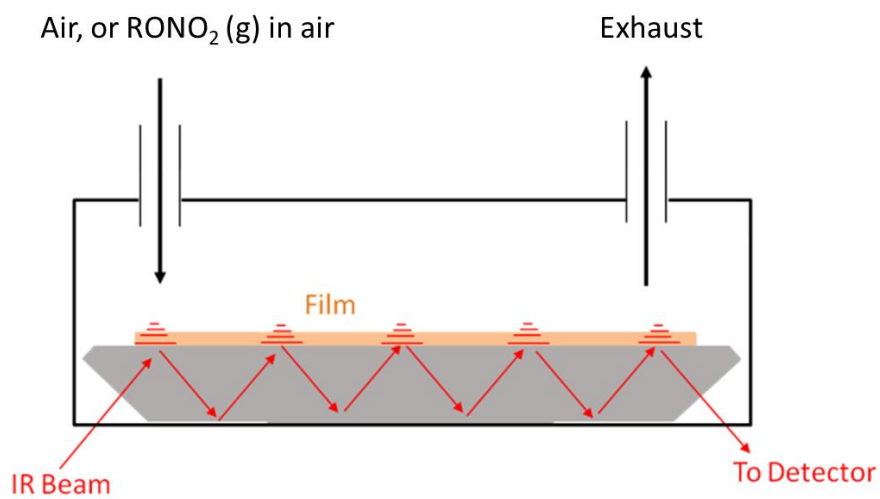


Figure 1: Structures of the organic thin film substrates triacontane (TC), poly(ethylene adipate) (PEA), pinonic acid (PA), and the gas phase organic nitrates β -hydroxyhexyl nitrate (HHN), β -hydroxypropyl nitrate (HPN), and 2-ethylhexyl nitrate (2EHN). SOA is not shown since it is a complex mixture.



28 **Figure 2:** Schematic of the ATR uptake apparatus.
29
30
31
32
33
34
35
36
37
38
39
40
41
42
43
44
45
46
47
48
49
50
51
52
53
54
55
56
57
58
59
60

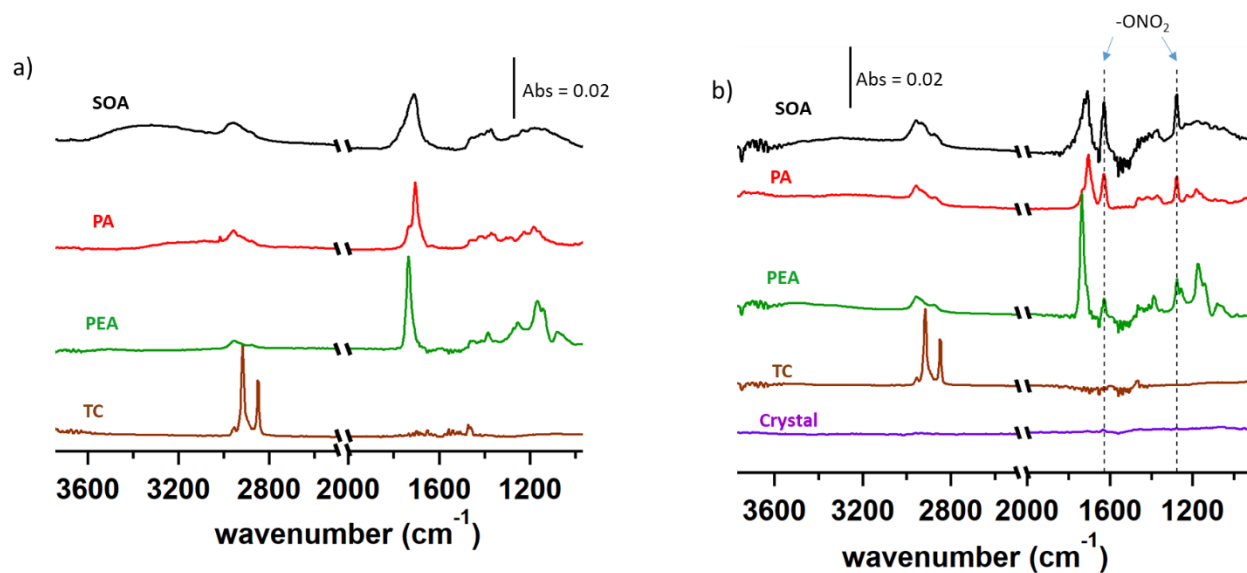


Figure 3: ATR- FTIR spectra for a) SOA, pinonic acid (PA), poly(ethylene) adipate (PEA), and triacontane (TC), and b) after exposure to gaseous HHN (5 ppm) once equilibrium was reached (450-1050 seconds), as well as the spectra for exposure of the clean crystal to the organic nitrate. All TC spectra were scaled by a factor of 0.25, and all PEA spectra by a factor of 0.5 to display them on the same scale as the other spectra. Dashed lines indicate the $-\text{ONO}_2$ signals characteristic of organic nitrates. The region between 2500-2000 cm^{-1} is not shown due to CO_2 (g) variation in the purge air.

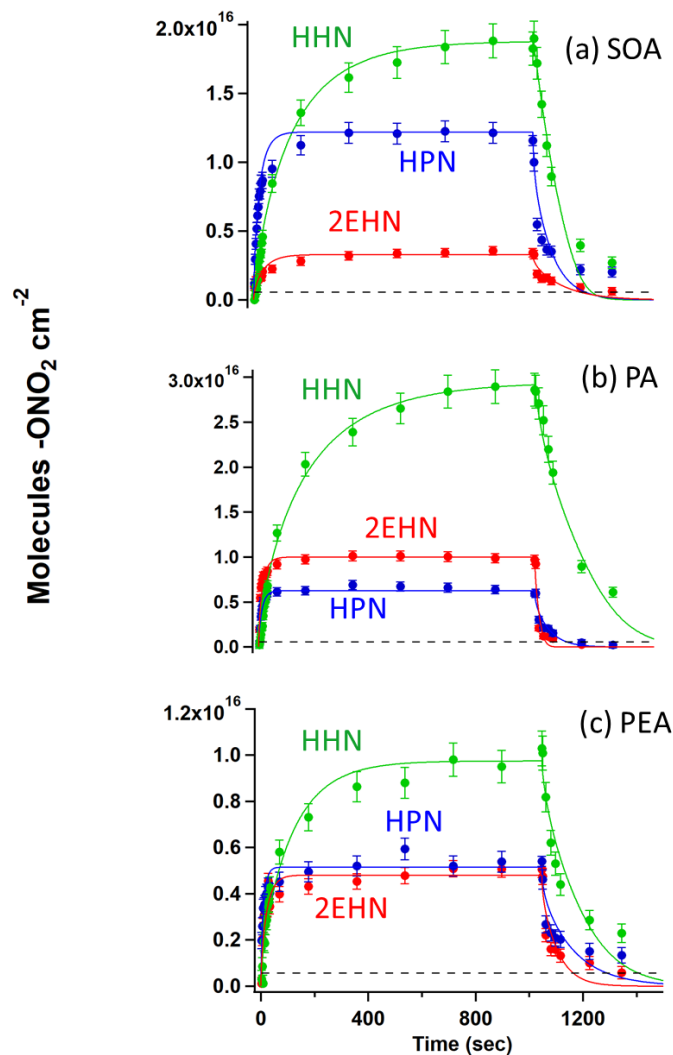


Figure 4: Concentrations of organic nitrates in molecules $-ONO_2 \text{ cm}^{-2}$ after exposure of (a) SOA, (b) PA and (c) PEA to gaseous HHN (5 ppm), HPN (250 ppm), and 2EHN (140 ppm). The dashed black line indicates the experimentally-determined limit of detection for the nitrates. Solid lines are best fits from the KM-GAP model. Error bars are $\pm 2\sigma$ on the experimental data points determined from the uncertainty in the measured absorption cross section of HHN, HPN and 2EHN.

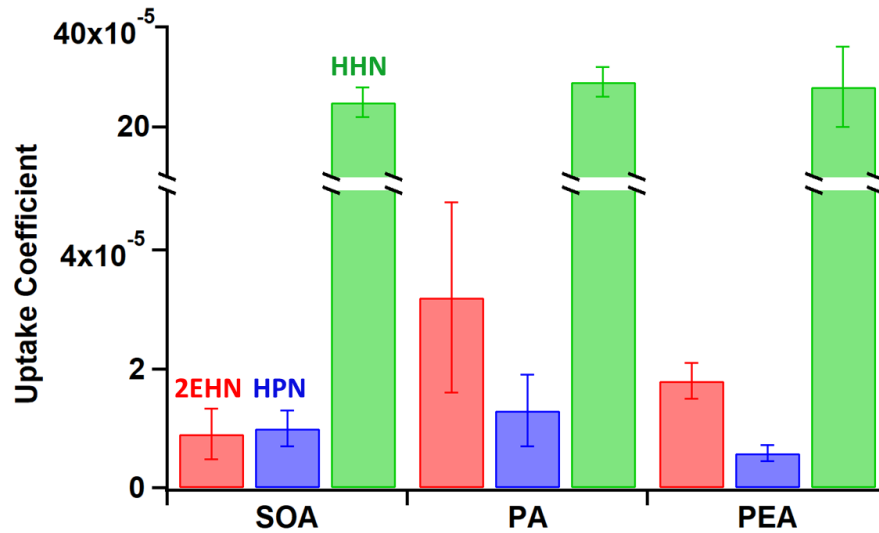


Figure 5: Initial uptake coefficients for the organic nitrates into SOA, PA, and PEA. The inset is rescaled to show 2EHN and HPN. Error bars are $\pm 1\sigma$ from the average of multiple experiments for each nitrate.

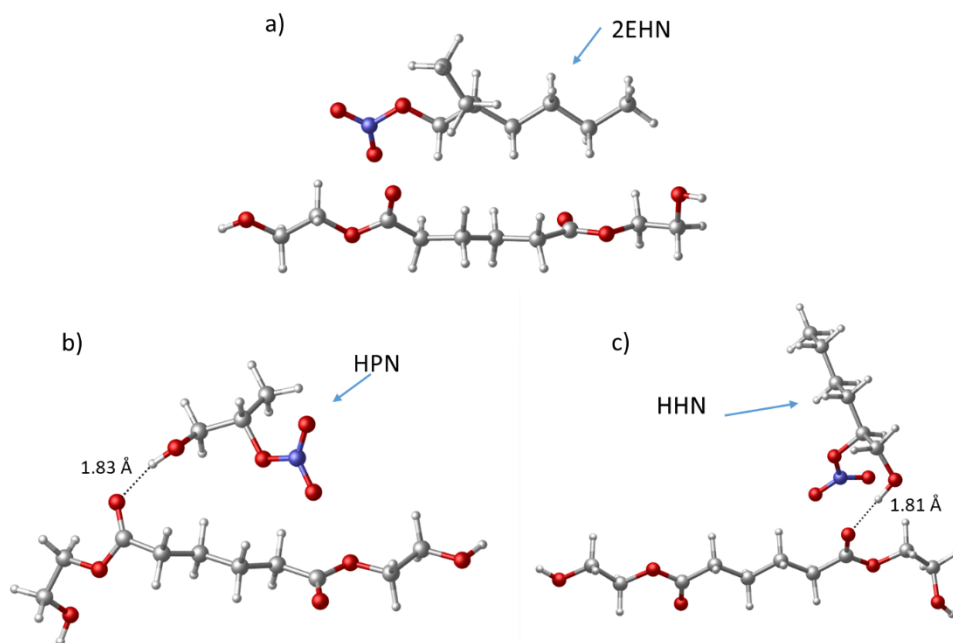


Figure 6: The optimized structure for a) one 2EHN molecule binding to one PEA subunit, b) one HPN molecule binding to one PEA subunit, and c) one HHN molecule binding to one PEA subunit. Hydrogen bonds are labeled with their bond length and bond angle.

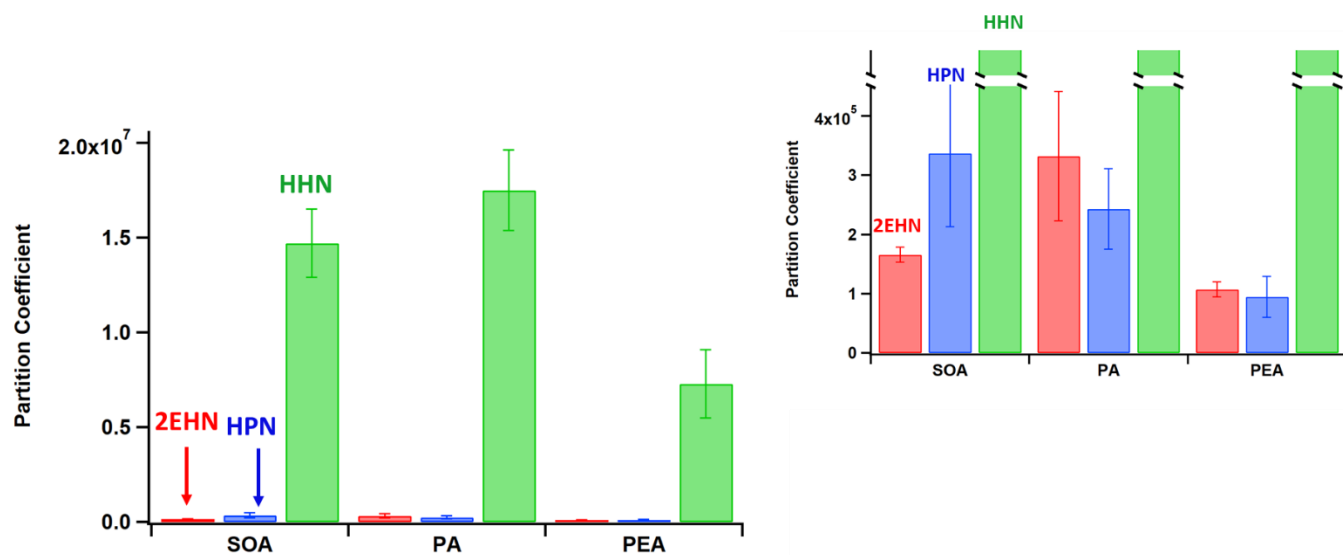


Figure 7: Equilibrium partition coefficients for the organic nitrates into SOA, PA, and PEA. The inset is rescaled to show 2EHN and HPN. Error bars are the statistical $\pm 1\sigma$ from the average of multiple experiments for each nitrate.

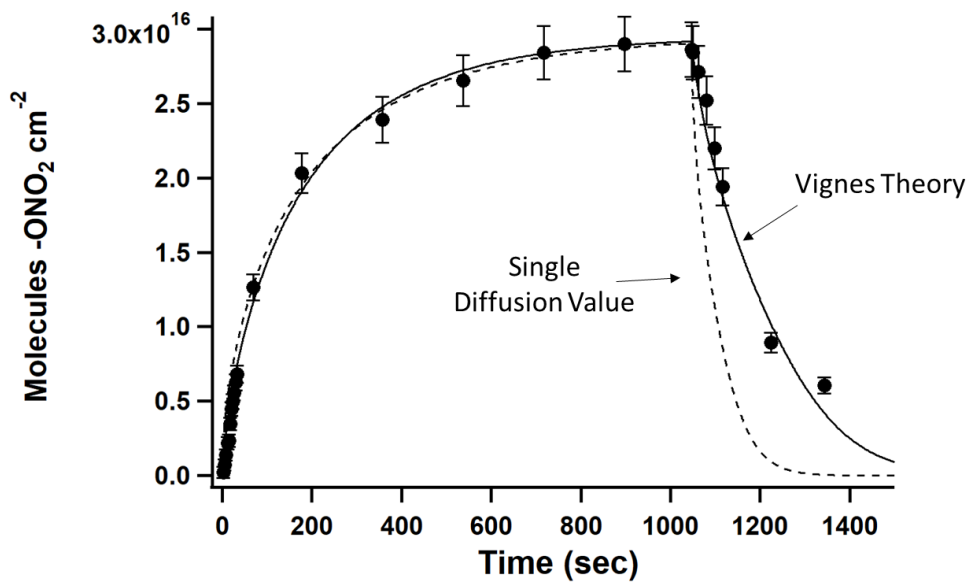


Figure 8: Uptake of HHN on PA. Points are the experimental data, where the error bars represent the uncertainty in the absorption cross section ($\pm 2\sigma$). The solid line shows the prediction from KM-GAP using a changing composition-dependent diffusion coefficient scenario with Vignes equations, while the dashed line shows the prediction using a constant composition-independent diffusion coefficient.

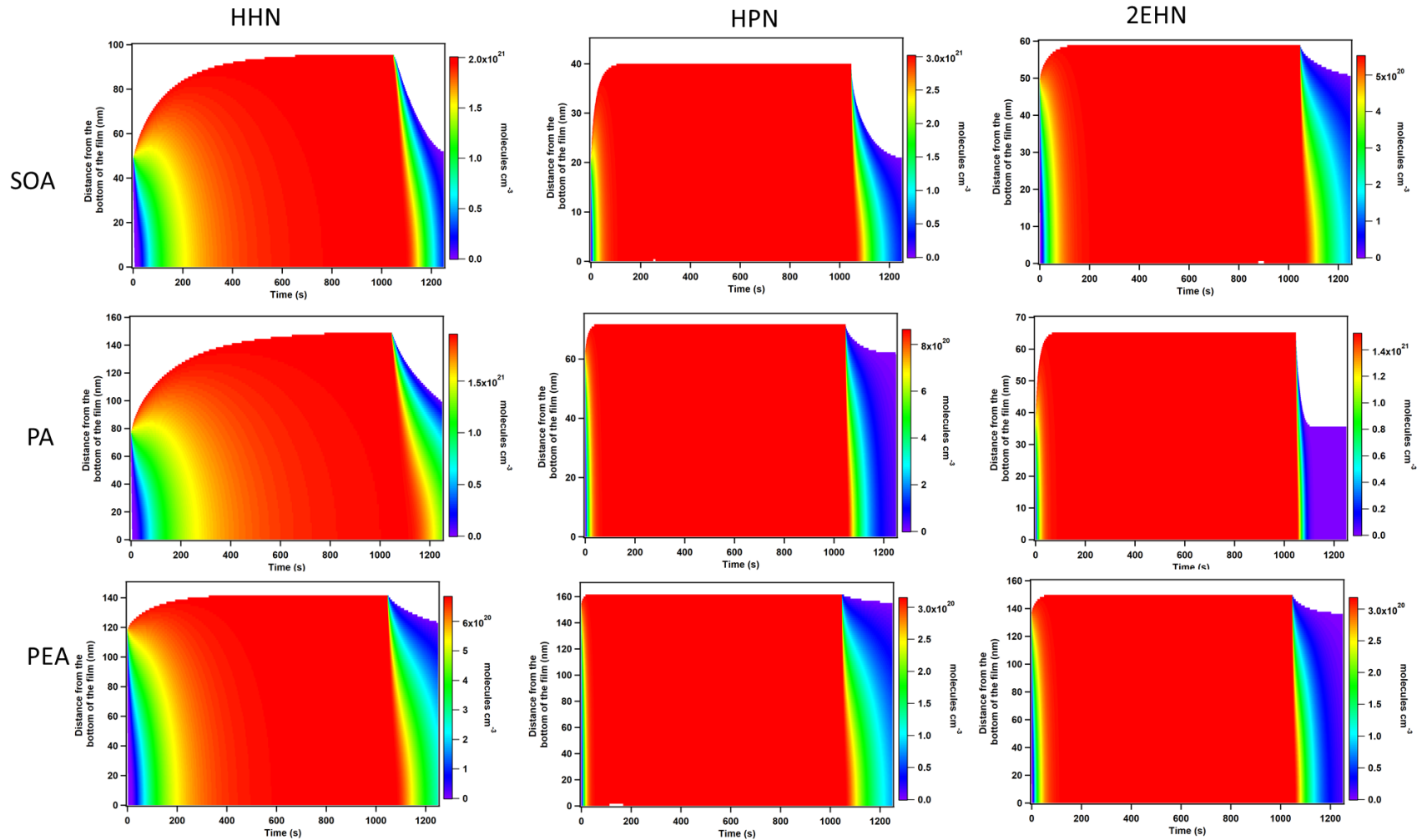


Figure 9: Contour plots for the organic nitrate concentrations in molecules cm^{-3} in the PA, PEA, and SOA films as a function of time and distance from the bottom of the film.

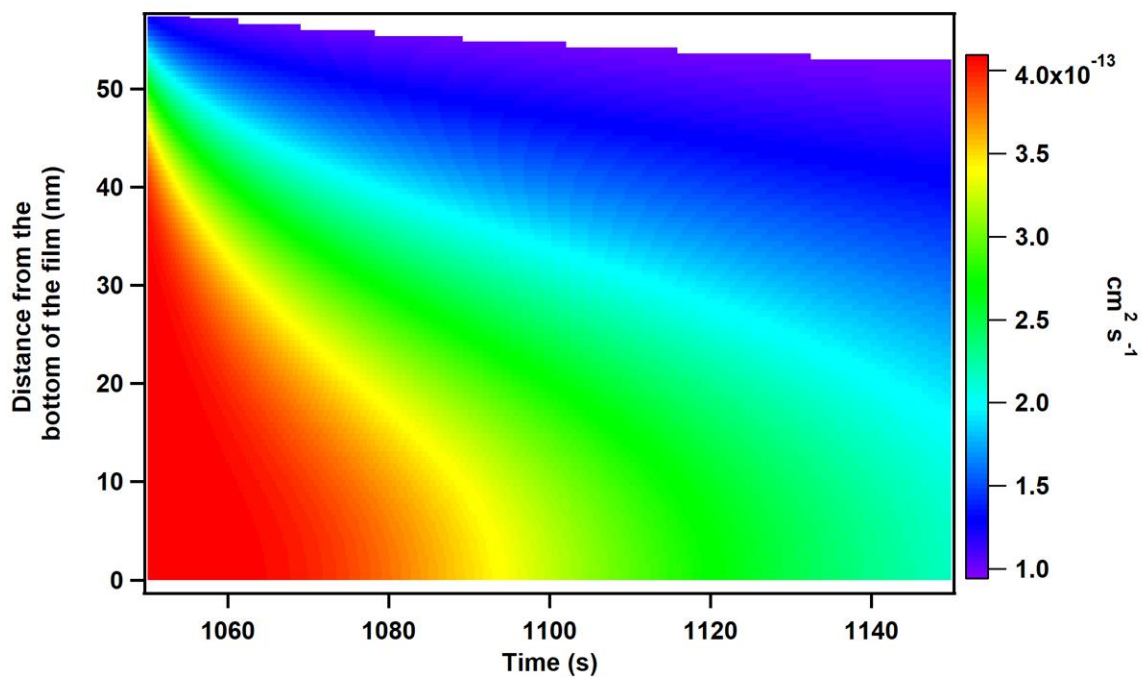


Figure 10: An expanded view of the diffusion coefficient contour plot for 2EHN on SOA.

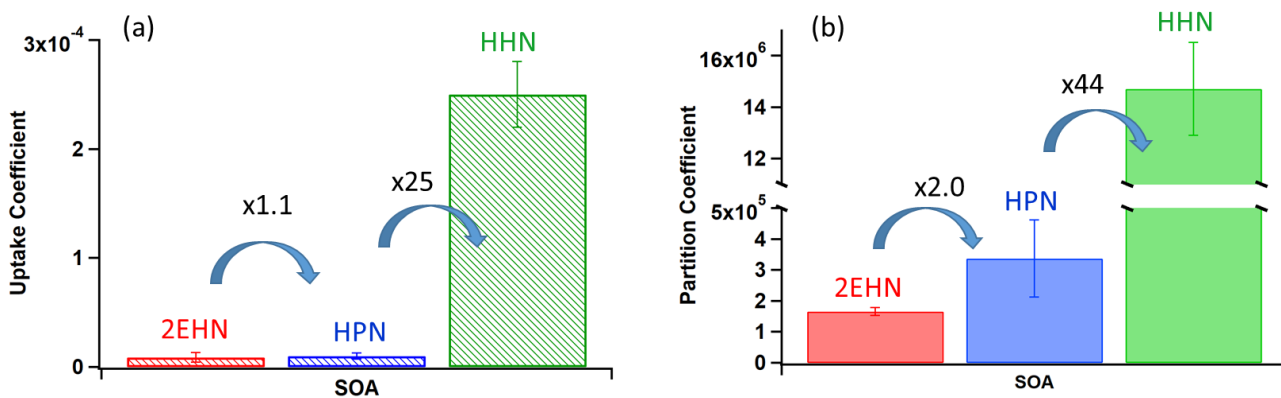


Figure 11: (a) Initial uptake coefficients and (b) equilibrium partition coefficients for all organic nitrates into SOA. Error bars are $\pm 1\sigma$ from the average of multiple experiments for each organic nitrate.

1
2
3 TOC: Experiments, kinetics modeling and quantum chemical calculations are combined to
4 probe both initial uptake and equilibrium partition coefficients for organic nitrates into various
5 organic films.
6
7
8
9
10
11
12
13
14
15
16
17
18
19
20
21
22
23
24
25
26
27
28
29
30
31
32
33
34
35
36
37
38
39
40
41
42
43
44
45
46
47
48
49
50
51
52
53
54
55
56
57
58
59
60

